

Manuscript Details

Manuscript number	MARGO_2017_112
Title	Baffin Bay Paleoenvironments in the LGM and HS1: Resolving the ice-shelf question
Article type	Research Paper

Abstract

Core HU2008029-12PC from the Disko trough mouth fan on the central West Greenland continental slope is used to test whether an ice shelf covered Baffin Bay during the Last Glacial Maximum (LGM) and at the onset of the deglaciation. We use benthic and planktic foraminiferal assemblages, stable isotope analysis of planktic forams, algal biomarkers, ice-rafted detritus (IRD), lithofacies characteristics defined from CT scans, and quantitative mineralogy to reconstruct paleoceanographic conditions, sediment processes and sediment provenance. The chronology is based on radiocarbon dates on planktic foraminifers using a ΔR of 140 ± 30 14C years, supplemented by the varying reservoir estimates of Stern and Lisiecki (2013) that provide an envelope of potential ages. HU2008029-12PC is bioturbated throughout. Sediments between the core base at 11.3 m and 4.6 m (LGM through HS1) comprise thin turbidites, plumites and hemipelagic sediments with Greenlandic provenance consistent with processes active at the Greenland Ice Sheet margin grounded at or near the shelf edge. Abundance spikes of planktic forams coincide with elevated abundance of benthic forams in assemblages indicative of chilled Atlantic Water, meltwater and intermittent marine productivity. IRD and IP25 are rare in this interval, but brassicasterol, an indicator of marine productivity reaches and sustains low levels during the LGM. These biological characteristics are consistent with a sea-ice covered ocean experiencing periods of more open water such as leads or polynyas in the sea ice cover, with chilled Atlantic Water at depth, rather than full ice-shelf cover. There is no supporting data for the existence of a full Baffin Bay ice shelf cover extending from grounded ice on the Davis Strait. Initial Greenland Ice Sheet retreat from the West Greenland margin is manifested by a pronounced lithofacies shift to bioturbated, diatomaceous mud with rare IRD of Greenlandic origin at 467 cm (16.2 cal ka BP; $\Delta R=140$ yrs) within Heinrich Stadial 1 (HS1). A spike in foraminiferal abundance and ocean warmth indicator benthic forams precedes the initial ice retreat from the shelf edge. At the end of HS1, IP25, brassicasterol and benthic forams indicative of sea-ice edge productivity increase, indicating warming interstadial conditions. Within the Bølling/Allerød interstadial a strong rise in IP25 content and IRD spikes rich in detrital carbonate from northern Baffin Bay indicate that northern Baffin Bay ice streams were retreating and provides evidence for increased open water, advection of Atlantic Water in the West Greenland Current, and formation of an IRD belt along the W. Greenland margin.

Keywords Arctic ocean and adjacent high latitudes; micropaleontology (forams); paleoceanography; Glacial sediments

Taxonomy Ice Sheets, Paleoceanography, Quaternary Stratigraphy

Corresponding Author Anne Jennings

Order of Authors Anne Jennings, John Andrews, Colm O'Cofaigh, Guillaume St-Onge, Simon Belt, Patricia Cabedo Sanz, Christof Pearce, Claude Hillaire-Marcel, Calvin Campbell

Suggested reviewers Leonid Polyak, Svend Funder, Richard Alley, Paul Knutz, Quentin Simon, Karen Luise Knudsen, Lev Tarasov

Submission Files Included in this PDF

File Name [File Type]

Margo_revision_letter_Jennings_8_15_17.doc [Response to Reviewers]

12PC LGM paper_8_4_2017_revision.docx [Revised Manuscript with Changes Marked]

Highlights.docx [Highlights]

12PC_MARGO_cleanvised_8_14_2017.docx [Manuscript File]

Fig.1_MG_rev.jpg [Figure]

Anne_jennings_figure2_revised.jpg [Figure]

Fig_3_12PCrev_mar_geol.jpg [Figure]

Fig_4.jpg [Figure]

Fig 5.jpg [Figure]

Fig_6rev_12PC_benthics_MGpaper.jpg [Figure]

Fig_7.jpg [Figure]

Table 1_MG.xlsx [Table]

To view all the submission files, including those not included in the PDF, click on the manuscript title on your EVISE Homepage, then click 'Download zip file'.

Research Data Related to this Submission

Data set

<https://data.mendeley.com/datasets/5c67tv7c74/draft?a=176055ec-dbe3-426c-a58d-05b30e1fe70a>

Data for: Baffin Bay Paleoenvironments in the LGM and HS1: Resolving the ice-shelf question

These data are for publication in Marine Geology for the special issue on Glaciated Continental Margins

1 Baffin Bay Paleoenvironments in the LGM and HS1: Resolving the ice-shelf 2 question

3
4 Anne E. Jennings^{1*}, John T. Andrews¹, Colm Ó Cofaigh², Guillaume St-Onge³, Simon
5 Belt⁴, Patricia Cabedo-Sanz⁴, Christof Pearce^{5,6}, Claude Hillaire-Marcel⁷, D. Calvin
6 Campbell⁸

7 ¹ INSTAAR University of Colorado, Campus Box 450, Boulder, CO 80309-0450 USA

8 ² Department of Geography, Durham University, South Road, Durham DH1 3LE, United
9 Kingdom

10 ³ Institut des sciences de la mer de Rimouski (ISMER) Université du Québec à Rimouski
11 and GEOTOP Rimouski, Québec, Canada S5L 3A1

12 ⁴ School of Geography, Earth and Environmental Sciences, University of Plymouth,
13 Plymouth PL4 8AA United Kingdom

14 ⁵ Department of Geological Sciences and Bolin Centre for Climate Research, Stockholm
15 University, Svante Arrhenius väg 8, SE-106 91 Stockholm, Sweden

16 ⁶ [Department of Geoscience and Arctic Research Centre, Aarhus University, Hoegh
17 Guldbergs gade 2, 8000 Aarhus, Denmark](#)

18 ⁷ Université du Québec a Montréal, Centre GEOTOP CP 8888, succ. Centre-Ville,
19 Montréal, Québec, Canada, H3C 3P8

20 ⁸ Geological Survey of Canada-Atlantic, Natural Resources Canada, Dartmouth Nova
21 Scotia

22 * anne.jennings@colorado.edu

23
24 Core HU2008029-12PC from the Disko trough mouth fan on the central West
25 Greenland continental slope is used to test whether an ice shelf covered Baffin Bay
26 during the Last Glacial Maximum (LGM) and at the onset of the deglaciation. We use
27 benthic and planktic foraminiferal assemblages, stable isotope analysis of planktic
28 forams, algal biomarkers, ice-rafted detritus (IRD), lithofacies characteristics
29 defined from CT scans, and quantitative mineralogy to reconstruct
30 paleoceanographic conditions, sediment processes and sediment provenance. The
31 chronology is based on radiocarbon dates on planktic foraminifers using a ΔR of 140
32 ± 30 ¹⁴C years, supplemented by the varying reservoir estimates of Stern and
33 Lisiecki (2013) that provide an envelope of potential ages. HU2008029-12PC is
34 bioturbated throughout. Sediments between the core base at 11.3 m and 4.6 m
35 (LGM through HS1) comprise thin turbidites, plumites and hemipelagic sediments
36 with Greenlandic provenance consistent with processes active at the Greenland Ice
37 Sheet margin grounded at or near the shelf edge. Abundance spikes of planktic
38 forams coincide with elevated abundance of benthic forams in assemblages
39 indicative of chilled Atlantic Water, meltwater and intermittent marine productivity.
40 IRD and IP₂₅ are rare in this interval, but brassicasterol, an indicator of marine
41 productivity reaches and sustains low levels during the LGM. These biological
42 characteristics are consistent with a sea-ice covered ocean experiencing periods of
43 more open water such as leads or polynyas in the sea ice cover, with chilled Atlantic
44 Water at depth, rather than full ice-shelf cover. They do not support the existence of
45 a full Baffin Bay ice shelf cover extending from grounded ice on the Davis Strait.
46 Initial ice retreat from the West Greenland margin is manifested by a pronounced
47 lithofacies shift to bioturbated, diatomaceous mud with rare IRD of Greenlandic
48 origin at 467 cm (16.2 cal ka BP; $\Delta R=140$ yrs) within HS1. A spike in foraminiferal
49 abundance and ocean warmth indicator benthic forams precedes the initial ice
50 retreat from the shelf edge. At the end of HS1, IP₂₅, brassicasterol and benthic

51 forams indicative of sea-ice edge productivity increase, indicating warming
52 interstadial conditions. Within the Bølling/Allerød interstadial a strong rise in IP₂₅
53 content and IRD spikes rich in detrital carbonate from northern Baffin Bay indicate
54 that northern Baffin Bay ice streams were retreating and provides evidence for
55 increased open water, advection of Atlantic Water in the West Greenland Current,
56 and formation of an IRD belt along the W. Greenland margin.

57
58 Keywords: Greenland Ice Sheet, Baffin Bay, paleoceanography, ice shelf,
59 foraminifera, Heinrich Stadial 1

60

61 **1. Introduction**

62

63 Last Glacial Maximum (LGM) climatic and oceanic conditions in Baffin Bay are
64 currently poorly known, but according to the temperature reconstructions from the
65 Greenland Ice Sheet borehole (Dahl-Jensen and al., 1998) and ice-core data (Buizert et
66 al., 2014), summit temperatures were ~20°C colder than present. Applying this
67 temperature difference down to sea level using the adiabatic lapse rate, suggests that the
68 annual temperature at the surface of Baffin Bay adjacent to Baffin Island would approach
69 -36°C. Such cold temperatures support the argument that cold-based ice covered the
70 forelands of eastern Baffin Island (Briner et al., 2003) with “Antarctic-like” conditions
71 across Baffin Bay, which would [also](#) suggest that Baffin Bay was covered in perennial
72 sea ice. At the LGM, confluent, Innuitian (IIS), Laurentide (LIS) and Greenland (GIS) ice
73 sheets (England et al., 2006) blocked the channels that connect Baffin Bay to the Arctic
74 Ocean (Dyke, 2002) and terminated in northern Baffin Bay as large ice streams (Li et al.,
75 2011; Blake, 1977). The Greenland ice sheet reached the continental shelf edge via large
76 ice streams off west Greenland (Ó Cofaigh et al., 2013a; Jennings et al., [in-revision2017](#);
77 Slabon et al., 2016; Sheldon et al., 2016; Dowdeswell et al., 2014), [but the outer limits of](#)
78 [the ice on the Baffin shelf are not known.](#)

79 On the basis of modeling, it has been proposed that Baffin Bay was blocked at its
80 southern end by an ice shelf extension of the Hudson Strait ice stream that grounded
81 across Davis Strait to reach southern Greenland, thus sealing Baffin Bay from the
82 Labrador Sea (Hulbe et al., 1997; Álvarez-Solas et al., 2010; Marcott et al., 2011). This
83 ice shelf was the starting point for modeling the processes that produce Heinrich events
84 (Hulbe et al., 1997; Álvarez-Solas et al., 2010; Marcott et al., 2011), but physical
85 evidence for it has not been recovered. An ice shelf of this scale would have
86 environmental consequences that should be recorded in Baffin Bay sediments. Firstly,
87 grounding of a Labrador Sea ice shelf along Davis Strait would prevent seawater
88 exchange between Baffin Bay and the Labrador Sea, excluding advection of organic
89 matter into Baffin Bay. It also would shut down *in situ* primary marine productivity in
90 Baffin Bay so that planktic and benthic organisms, their biomarkers, and bioturbation
91 would be absent in the sediment. Secondly, ice shelves and even extensive sea-ice cover
92 are known to restrict the movement and export of icebergs (Reeh et al., 2001; Domack
93 and Harris, 1998). Thus iceberg rafting and mixing of sediments of various provenances
94 in Baffin Bay would be reduced. Using these concepts, we test the LGM Baffin Bay ice-
95 shelf hypothesis by studying the sedimentological and biological characteristics of
96 sediments in HU2008029-12PC from the continental slope off western Greenland, a core
97 that extends from the LGM into the Younger Dryas (YD) and that recorded retreat of the
98 Greenland Ice Sheet during deglaciation (Jennings et al., [in-revision2017](#)).

99

100 **2. Setting of core HU2008029-12PC**

101 Detailed studies of LGM and deglacial environments in Baffin Bay have been hampered
102 by relatively slow sediment accumulation rates and poor calcium carbonate preservation
103 (cf. Aksu, 1985; de Vernal et al., 1992; Simon et al., 2012). HU2008029-12PC (hereafter
104 called 12PC) was raised from the northern side of the Disko trough mouth fan (TMF)
105 from acoustically stratified sediments with continuous parallel reflections on the eastern
106 side of Baffin Bay (68°13.69' N; 57°37.08' W; 1475 m water depth; Campbell and de
107 Vernal, 2009) (Figs. 1 and 2). This site on the trough mouth fan has higher sediment
108 accumulation than sites in the deep basin of Baffin Bay [that have variable sedimentation](#)
109 [rates that range between 3 and 35 cm/ka](#) (Andrews et al., 1998; Hillaire-Marcel et al.,
110 1989, 2004; Simon et al., 2012; 2014) (Fig. 1).

111 The Disko TMF was built throughout the Quaternary by rapid sediment
112 deposition in front of the fast flowing Disko ice stream (Fig. 1) when the GIS margin was
113 extended on the shelf, and from hemipelagic sedimentation during and after ice retreat
114 (ÓCofaigh et al., 2013a, b; Jennings et al., [in-revision2017](#); Hofmann et al., 2016). An
115 ice sheet grounded at or near the shelf edge delivers abundant sediments directly to the
116 continental slope in the form of sediment gravity flows, including turbidity currents that
117 form graded sand layers, stratified sand/silt beds, and glacial debris flows (ÓCofaigh
118 et al., 2013a, b, Lucci and Rebesco, 2007). Turbid meltwater plumes released from the
119 ice front produce plumites, which are finer grained than the turbidites as the sand is
120 dropped near the ice front and the silt and clay continue offshore in suspension (Hesse et
121 al., 1997; Lucchi and Rebesco, 2007). Depending on sea surface conditions such as
122 perennial sea ice and/or ice shelves, icebergs would also deliver sediment to the slope as

123 they melted during their transit in Baffin Bay (Andrews et al., 1998; 2014; Jennings et al.,
124 2014; Simon et al., 2012; 2014; [2016](#); Sheldon et al., 2016).

125 ~~Each year, the~~[The](#) modern sea ice edge extends southeast to northwest within
126 Baffin Bay and sea ice cover is greater in the western than in the eastern half due to the
127 influence of the relatively warm and saline West Greenland Current that enters Baffin
128 Bay from the southeast (Tang et al., 2004; Münchow et al., 2015) (Fig. 1). The boundary
129 between lower salinity, sea-ice bearing, Arctic Surface Water (ASW) that passes from the
130 Arctic Ocean through the channels of the Canadian Arctic Archipelago into Baffin Bay
131 and Atlantic Waters of the West Greenland Current (WGC) moving northward along
132 West Greenland is oriented NE-SW and migrates through the year. The relatively warm,
133 saline Atlantic Water submerges beneath the ASW (Buch, 2000a, b) and forms the West
134 Greenland Intermediate Water (WGIW) (Fig. 1 inset) (Tang et al., 2004). During the
135 LGM, however, the circulation regime in Baffin Bay would have been different because
136 the southward flow of ASW into Baffin Bay was blocked by confluent ice sheets
137 grounded in the channels of the Canadian Arctic Archipelago until the early Holocene
138 (England, 1999; Zreda et al., 1999; Jennings et al., 2011a; Pińkowski et al., 2011).
139 Today, warm Atlantic Water carried in the WGC accesses the GIS margins via cross
140 shelf troughs and fjords, where the ice sheet terminates in the sea (Holland et al., 2008)
141 and promotes basal melting (Straneo et al., 2012). WGC Atlantic Water flow was
142 initiated as early as 14.4 cal ka BP off central West Greenland and is implicated in
143 Greenland Ice Sheet retreat from the LGM position at the shelf edge (cf. Knutz et al.,
144 2011; Sheldon et al., 2016; Jennings et al., [in-revision2017](#)).

145

146 **3. Methods:**

147 3.1 Age Model

148 The age model for 12PC is based on 7 radiocarbon dates between 201 and 860 cm on the
149 arctic planktic foraminifer, *Neogloboquadrina pachyderma* (*sensu* Darling et al., 2006).

150 The dates were previously published in Jennings et al., (~~in revision~~2017) (Table 1).

151 Radiocarbon dates were calibrated using the Marine13 curve (Reimer et al., 2013). OxCal
152 version 4.2.4 (Ramsey and Lee, 2013) was used to compute an age/depth model (Fig. 3).

153 An age reversal in the upper 110 cm of the core limited the chronology to the interval
154 from 200 cm to the base of the core (1130 cm). The age of the core base is assumed to be

155 no older than 26.5 ka BP, the beginning of the LGM (Clark et al., 2009). This assumed

156 basal age results in a large uncertainty in the modeled age of the base of the core (24 to

157 28 cal ka BP). Given this basal age, we might expect to record Baffin Bay Detrital

158 Carbonate (BBDC) event BBDC3 that is found in central Baffin Bay from c. 23.5 to 25

159 cal ka BP (Simon et al., 2016). A single data point with 20% NBB source at 21.5 cal ka

160 BP may represent BBDC2 (21 cal ka BP; Simon et al., 2016) although it is not associated

161 with a coarse clast-rich interval as would be expected if it represented a BBDC event

162 (Andrews et al., 1998; Simon et al., 2012; Jackson et al., 2017) (Fig. 3). The lack of an

163 interval of high NBB and IRD below 467 cm (16.2 cal ka BP) in 12PC indicates that

164 BBDC2 and BBDC3 were not recovered in 12PC. Either these two events were not

165 deposited basin wide or the basal age of 12PC is younger than the 21 ka BP age of

166 BBDC2. Given that the deepest radiocarbon age in 12PC is 21.8 cal ka BP ($\Delta R=140$

167 years) and there are 3 meters of sediment below this depth in the core, we suggest it is

168 more likely that BBDC2 and 3 were not deposited basin wide. Without additional

169 [information we continue with the assumption that the core base is no older than the](#)
170 [beginning of the global LGM of 26.5 ka BP \(Clark et al., 2009\).](#)

171 ~~lack in core 12PC of Baffin Bay Detrital Carbonate (BBDC) events BBDC2 and~~
172 ~~BBDC3, deposited between 24.7 to 25 cal ka BP and 26.4 to 27.7 cal ka BP, respectively~~
173 ~~(Simon et al., 2014).~~ We initially built the age model assuming a marine reservoir offset
174 (ΔR) of 140 ± 30 years based on recent work in Disko Bugt (Lloyd et al., 2011), for
175 consistency with other central West Greenland sediment core records (cf Jennings et al.,
176 2014; ~~in revision~~2017; Jackson et al., 2017; Hogan et al., 2016; Sheldon et al., 2016), and
177 we note that prior to 2011, many publications used a $\Delta R=0$ [years](#) (Andrews et al., 1998;
178 Knudsen et al., 2008). However, recognizing that the marine reservoir offset could be
179 large and variable over the time interval of 12PC and because this core extends into the
180 LGM, [defined here as beginning at 26.5 ka \(Clark et al., 2009\) and ending at the](#)
181 [beginning of the Oldest Dryas period, 18 ka BP \(Buizert et al., 2014\)](#), we used the
182 variable North Atlantic R values in Stern and Lisiecki (2013) to provide an envelope of
183 calibrated age so that we could consider the correlations of boundaries and conditions
184 recorded in the core with established climatic intervals (Fig. 3f). To accomplish this we
185 first calibrated each date with $\Delta R=0$ ^{14}C years, which provides the maximum age. We
186 then used the $\Delta R=0$ ages to identify the appropriate 500 year bin of maximum, average
187 and minimum R values from Table S1 of Stern and Lisiecki (2013) and calibrated each of
188 the dates using these three R-values. The resulting envelope of ages, from $\Delta R=0$ to the
189 maximum Stern and Lisiecki 2013 R-value, illustrates how the choice of ΔR affects
190 correlation of boundaries in the core with climate intervals from LGM through the YD
191 (Fig. 3f; Table 1). Regardless, these results confirm that the core contains LGM and

192 Heinrich Stadial 1 (aka Oldest Dryas) sediments, a key requirement for testing the ice
193 shelf model (Hulbe et al., 1997; Álvarez-Solas et al., 2010; Marcott et al., 2011).

194

195 3.2 Foraminiferal analyses.

196 One-cm wide samples were weighed wet and sieved on a 63- μm screen. Material >63
197 μm was kept wet in a storage solution of 70% distilled water and 30% ethanol with
198 baking soda as a buffer. Foraminifera were counted wet to prevent destruction of fragile
199 tests that disintegrate under the stress of drying. A wet splitter was used when necessary
200 to achieve a count of 200-300 benthic foraminifers and as many planktic foraminifers
201 as were in the benthic split. In most cases the full sample was counted. Equivalent dry
202 weights of the foram samples were estimated from sedimentology samples from the same
203 depths that had both wet and dry weights, allowing foraminifera/gram sediment to be
204 calculated.

205

206 3.3 Stable isotope analyses

207 Stable oxygen and carbon isotopes were measured on the planktic foram species
208 *Neogloboquadrina pachyderma* picked from the 150-250 μm size fraction in 41 samples;
209 results from 3 samples were rejected because they yielded a low signal. Samples $>100 \mu\text{g}$
210 have standard deviations of 0.01 and 0.03 ‰ for $\delta^{13}\text{C}$ and $\delta^{18}\text{O}$ respectively. Samples
211 weighing $<100 \mu\text{g}$ are reported with a standard deviation of 0.06 ‰ for $\delta^{13}\text{C}$, and an error
212 of ± 0.2 ‰ for $\delta^{18}\text{O}$. The oxygen isotope values are expressed as ‰ vs VPDB. Between
213 1050 and 857 cm all samples were of small weight but otherwise seemed reliable.
214 Measurements were made on a Micromass Isoprime™ dual inlet coupled to a

215 MulticarbTM system at the Light Stable Isotope Geochemistry Laboratory at the
216 University of Montréal – UQAM.

217

218 3.4 CT scan.

219 CT scanning of the half round core was performed at the sediment core laboratory at the
220 University of Quebec at Rimouski. A CT number (a measure of sediment density) was
221 extracted from the images. The CT scan image was used to determine lithofacies and
222 boundaries, sedimentary structures, and to identify bioturbation, a key source of evidence
223 for the presence of benthic organisms and a source of information about sedimentation
224 rate variations between the radiocarbon dates (Wetzel, 1991). Counts of >2 mm clasts
225 interpreted as ice rafted detritus (IRD) were made from the CT images by counting in a 2
226 cm wide window across the core width continuously along the core length (Grobe, 1987).

227

228 3.5 Biomarkers: IP₂₅ and Brassicasterol

229 Biomarker analyses (IP₂₅ and brassicasterol) were performed using methods described
230 previously (Belt et al., 2012; Belt et al., 2015). Briefly, 9-octylheptadec-8-ene (9-OHD,
231 10 µL; 10 µg mL⁻¹) and 5 α -androstane-3 β -ol (10 µL; 10 µg mL⁻¹) were added to ca. 1 – 2
232 g of each freeze-dried sediment sample prior to extraction to permit quantification of IP₂₅
233 and sterols, respectively. Samples were then extracted using dichloromethane/methanol
234 (3 x 3 mL; 2:1 v/v) and ultrasonication. Following removal of the solvent from the
235 combined extracts using nitrogen, the resulting total organic extracts (TOE) were purified
236 using column chromatography (silica) with IP₂₅ (hexane; 6 mL) and brassicasterol (20:80
237 methylacetate/hexane; 6 mL) collected as two single fractions. Non-polar lipid fractions

238 were further separated into saturated and unsaturated hydrocarbons using glass pipettes
239 containing silver ion solid phase extraction material (Supelco Discovery® Ag-Ion).
240 Saturated hydrocarbons were eluted with hexane (1 mL), while unsaturated hydrocarbons
241 (including IP₂₅) were eluted with acetone (2 mL). All fractions were dried under a stream
242 of nitrogen.

243 Analysis of individual fractions was carried out using gas chromatography - mass
244 spectrometry (GC-MS) with operating conditions as described previously (e.g. Belt et al.,
245 2012; Brown and Belt, 2012). Sterols were derivatized (BSTFA; 50 µL; 70 °C; 1 h) prior
246 to analysis by GC-MS. Mass spectrometric analysis was carried out in total ion current
247 (TIC) and single-ion monitoring (SIM) modes. Individual lipids were identified on the
248 basis of their characteristic GC retention indices and mass spectra obtained from
249 standards. Quantification of IP₂₅ was achieved by dividing its integrated GC-MS peak
250 area by that of the internal standard (9-OHD) in SIM mode (both *m/z* 350) and
251 normalizing this ratio using an instrumental response factor (obtained from laboratory
252 standards of each analyte) and the mass of sediment (Belt et al., 2012). Analytical
253 reproducibility (6 %, n = 3) was monitored using a sediment with a known concentration
254 of IP₂₅. Brassicasterol concentrations were obtained by comparison of their respective
255 peak areas in SIM mode (brassicasterol, *m/z* 470) with those of the internal standard (*m/z*
256 333) and normalized as per IP₂₅.

257

258 3.6 Quantitative X-ray diffraction Mineralogy

259 Quantitative x-ray diffraction (qXRD) analyses were used to identify shifts in sediment
260 sources between ~~more~~ 'local' West Greenland (WG) and 'distal' Northern Baffin Bay

261 (NBB). Samples for qXRD analysis were taken at 10 to 20 cm intervals throughout the
262 core. Sediment samples were freeze-dried and processed at INSTAAR using the method
263 described by Eberl (2003) and Andrews and Eberl (2011). The qXRD samples were
264 analysed on a Siemens D5000 XRD unit at a 0.02 2- θ step with a 2 second count;
265 minerals were identified using the program RockJock v.6 (Eberl, 2003). The qXRD 2-
266 source data to 17.5 cal ka BP is presented in Jennings et al. ([in-revision2017](#)). The
267 determination of sediment provenance is based on the quantitative X-ray diffraction
268 (qXRD) analysis of the < 2 mm surface and core sediments using the method outlined by
269 Eberl (2003) and described in more detail for our area by (Andrews and Eberl, 2012;
270 Andrews et al., 2014; O'Cofaigh et al., 2013a; [Simon et al., 2014](#)). We use the Excel
271 macro unmixing program "[SedUnMix](#)" (~~first described by Eberl (2004), 2004; Andrews~~
272 ~~and Eberl, 2012) to~~ [and developed further by Andrews and Eberl \(2012\) to](#) ascribe
273 sediment mineral assemblages to probable source areas. In this present study we
274 discriminated between two glacial derived sources; first a regional West Greenland
275 source dominated by specific ranges in quartz, plagioclase, k-feldspars and other non-
276 clay and clay minerals, versus a North Baffin Bay detrital carbonate source [dominated by](#)
277 [dolomite](#) (Andrews et al., 2014; O'Cofaigh et al., 2013; Jennings et al., [in-revision2017](#)).

278

279 **4. Results [and Interpretation](#)**

280 4.1 Lithofacies Characteristics

281 There are two main lithofacies units defined by the sediment parameters in 12PC
282 (Fig. 3). The boundary between the two units (Fig. 4b) is well expressed by an abrupt
283 shift to lower CT# (Fig. 3A). This transition dates to 16.2 cal ka BP using $\Delta R=140$ years

284 and has been interpreted to represent the retreat of the Greenland Ice Sheet from the shelf
285 edge (Jennings et al., [in-revision2017](#)). However, the full age-envelope ranges between
286 16.4 ($\Delta R=0$) to 14.0 (Max R) ka, or, late in Heinrich Stadial 1 to the end of the Bølling
287 (Fig. 3f). Calibrated radiocarbon dates (Fig. 3F; $\Delta R=140$, pink) in the lower unit range
288 from 21.8 to 16.2 cal ka BP. The lower three radiocarbon dates fall within the LGM
289 regardless of the marine reservoir age selected (Fig. 3F). The radiocarbon date at 571.5
290 cm falls within Heinrich Stadial 1 regardless of the marine reservoir age (Fig. 3F).

291 The lower lithofacies unit, which represents the period when the ice sheet
292 grounding line was at or near the shelf edge, has higher magnetic susceptibility (Fig. 3C),
293 [higher-variable](#) sand content [including high weight percentage peaks](#) (Fig. 3D) and a west
294 Greenlandic sediment composition (Fig. 3E) but rare >2mm clasts (Fig. 3B). From the
295 base of the core to 1022 cm, sediments are laminated mud with straight, sharp contacts
296 defining the laminae and vertically oriented burrows (Fig. 4f). Between 1025 and 768 cm
297 the sand content increases and stratification is disrupted by bioturbation (Fig. 3E).
298 Stratified mud with distinct vertical burrows extends from 768 to 735 cm (Fig. 3D). From
299 735 cm to 688 cm sand content increases. This sandy unit is overlain by another
300 sequence of stratified mud with distinct burrows between 688 and 630 cm. The sediment
301 between 630 and 467 cm is bioturbated, stratified mud with layering disturbed by
302 bioturbation (Fig. 4c). The uppermost part of this unit has high sand content and marks
303 the transition to the upper lithofacies unit.

304 The upper lithofacies from 467 to 0 cm, which represents deglaciation [and the](#)
305 [Holocene](#) (Jennings et al., [in-revision2017](#)), has overall lower CT number (lower density)
306 (Fig. 3A), lower magnetic susceptibility (Fig. 3C) and [generally](#) lower sand content (Fig.

307 3D). But, it has much higher numbers of >2mm clasts (IRD) (Fig. 3B). Immediately
308 above the boundary the sediments are low-density bioturbated mud with the sand fraction
309 comprising *Coscinodiscus* planktic diatoms and setae of *Chaetoceras*, consistent with the
310 low MS values (Fig. 3c). Well-defined, thin laminae and rare IRD occur at the base of the
311 unit, but transition upward to less-well defined laminae and rare to absent IRD from 420
312 cm to 352 cm. This fine interval was interpreted to record a period in the initial
313 deglaciation as the grounding line retreated off the shelf edge with retention of an ice
314 shelf (Jennings et al., [in-revision2017](#)). At 352 cm ([marked by middle horizontal blue line](#)
315 [on Figure 3](#)) the CT # (density), MS and sand increase ~~and a spike in Greenlandic IRD~~
316 ~~occurs at 330 cm~~ (Fig. [3A, B, C, DE](#)). This level marks the start of renewed retreat of
317 the GIS grounding line by calving (Jennings et al., [in-revision2017](#)). The sediments are
318 bioturbated but stratification is still evident, suggesting moderate sedimentation rates.

319 ~~Apart from a peak in >2mm clasts of west Greenland provenance at 330 cm~~ The CT#, MS
320 ~~and sand values increase to moderate levels at 355 cm (Fig. 3A, B, C) but the main rise in~~
321 ~~>2mm clasts coincides with the entry of the~~ and Northern Baffin Bay sediment source
322 (NBB source) ~~content do not increase until~~ at 290 cm (Fig. 3B, E). ~~The relatively low MS~~
323 ~~is consistent with the high detrital carbonate content of the NBB source (Fig. 3C, E).~~

324 Bioturbated, pebbly mud associated with a rise in NBB provenance occurs between 280
325 and 175 cm with the highest IRD interval from 280-240 cm (Fig. 3B, E). This NBB DC
326 interval has been found in several cores on the central West Greenland slope (Sheldon et
327 al., 2016; Jennings et al., [in-revision2017](#); [Jackson et al., 2017](#)) and has been correlated to
328 BBDC1 (Simon et al., 2012; 2014; [Jackson et al., 2017](#)), marking the retreat of NBB ice
329 streams. The NBB DC event is overlain by bioturbated mud with small, dispersed IRD

330 and discontinuous silt stringers between 175 and 152 cm. Bioturbated pebbly mud
331 between 152 and 52 cm has high NBB provenance between 160 and 90 cm, an interval
332 that contains an age reversal and a mixture of radiocarbon ages (Fig. 3F). The age
333 reversal suggests that the upper NBB peak is reworked. The upper 52 cm of the core is
334 bioturbated mud with dispersed IRD likely represents the middle to late Holocene time
335 period, although it is undated.

336

337 4.2 Biological Proxies

338 Biological proxy data are expressed against age using the age model based on $\Delta R=140$
339 yrs (Fig. 5).

340 4.2.1 Bioturbation

341 The CT scan image (Fig. 3) reveals that the entire core is bioturbated, except for
342 one short interval in the LGM from 974 to 1005 cm, indicating that there was sufficient
343 oxygenation and food to support the benthos in Baffin Bay throughout the time period
344 represented by the core (Löwemark et al., 2012). Variations in burrow shape and density
345 are indicative of the interplay between oxygenation, sedimentation rate, sedimentation
346 processes, substrate consistency and food supply (Reineck and Singh, 1980, Wetzel,
347 1991; Löwemark et al., 2012) (Fig. 4). Intensely bioturbated intervals in which sand
348 layers are disrupted by burrowing (e.g. Fig. 4a, c, e) suggest periods of relatively slow
349 sedimentation (Wetzel, 1991), whereas intervals of vertical burrows terminated by
350 overlying strata (e.g. Fig. 4d, f) indicate episodic rapid sedimentation (Jennings et al.,
351 2011a). Figure 4 shows expanded views of segments of the CT image shown in full on
352 Figure 3 to illustrate some of the key lithofacies characteristics and trace fossil types that

353 provide evidence for sedimentation processes. Muddy intervals typically have vertical
354 burrows that are truncated by subsequent strata (Fig. 4d). These mud intervals likely
355 represent plumites deposited from turbid meltwater plumes, whereas the sandy, stratified
356 intervals with varying degrees of bioturbation likely represent distal turbidites (Ó Cofaigh
357 and Dowdeswell, 2001) (Fig. 4c, f).

358 4.2.2 Foraminifera and Stable Isotopes

359 The Foraminiferal abundances in 12PC are spiky, with intervals of low benthic and
360 planktic numbers per gram of dry sediment punctuated by periods of much higher
361 numbers of foraminifers per gram (Fig. 5D). The high variability in abundance relates to
362 variations in marine productivity, overprinted by carbonate dissolution, and dilution by
363 high (12.8 cm/ka on average from 250-860 cm) and varying sedimentation rates. The
364 lithofacies characteristics suggest widely varying sedimentation rates in the core that are
365 not captured by the less frequent age control. Therefore we did not attempt to calculate
366 foraminiferal flux, which would have been a more direct measure of productivity, but
367 rather rely on foraminiferal numbers per gram as a measure of productivity.

368 *N. pachyderma*, the only planktic species, forms abundance spikes up to 1620
369 specimens/g, with intervening periods of very low abundance to absence (Fig. 5). The
370 planktic forams were quite small from the base of the core to 860 cm (22 cal ka BP), but
371 increased in size above that level. In general the planktic and benthic foram abundances
372 rise and fall together, suggesting that the abundance spikes represent *in situ* productivity
373 and a link between surface productivity and benthic food supply, although we cannot
374 control for variations in carbonate preservation. Low numbers of *N. pachyderma* per
375 gram are consistent with low productivity under perennial sea ice and the high numbers

376 per gram are consistent with periods of more open water, such as leads or polynyas in
377 summer (e.g. Nørgaard-Pedersen et al., 2003). Advection of planktic foraminifers from
378 outside Baffin Bay is unlikely, especially given the linkage between the benthic and
379 planktic productivity (cf Knutz et al., 2011; Nørgaard-Pedersen et al., 2003).

380 Oxygen isotope values on *N. pachyderma* ranged between 5.4 and 2 ‰. The
381 interval between 22 and 18.2 cal ka BP has mostly heavy values that fall between 4 and 5
382 ‰ (Fig. 5), comparable to MIS 2 values in the Fram Strait (Nørgaard-Pedersen et al.,
383 2003). A shift to lighter $\delta^{18}\text{O}$ and $\delta^{13}\text{C}$ values begins at 18 cal ka BP, suggests reduced
384 ventilation (Sarnthein et al., 1995). This interval falls within HS1 regardless of which ΔR
385 is applied (Fig. 2; Table 1). Above this shift the $\delta^{18}\text{O}$ values remain above 3.7 ‰. A
386 pronounced light $\delta^{18}\text{O}$ spike at 19.4 cal ka BP corresponds to high planktic abundance
387 and increased IP₂₅ and Brassicasterol (Fig. 5). Oxygen isotopic values of this magnitude
388 can either be related to glacial meltwater, especially if they are paired with light $\delta^{13}\text{C}$
389 values (Sarnthein et al., 1995) or to increased rate of sea-ice production that can produce
390 brines with a light isotopic signature (Hillaire-Marcel et al., 2004; Hillaire-Marcel and de
391 Vernal, 2008). The overall trend in the $\delta^{13}\text{C}$ values is toward heavier values suggesting
392 better ventilation at the top of the record than at the bottom (Fig. 5).

393 The benthic foraminiferal assemblages (Fig. 6) provide insights into the
394 productivity of surface waters, stratification of the water column, and turbid glacial
395 meltwater influx. For example, sea-ice edge migration, either seasonal or in the form of
396 leads or polynyas, produces pulses of phytoplankton production that sink to the seabed,
397 providing food for benthic communities. The three most common benthic foraminiferal
398 species in 12PC are *Stainforthia feylingi*, *Cassidulina reniforme* and *Elphidium*

399 *excavatum* forma *clavata*. *S. feylingi* is dominant in conditions of stratified water column
400 with a cold freshwater lid and has been associated with productivity at the seasonal sea
401 ice edge (Seidenkrantz, 2013). It has been found in high abundances associated with
402 biosiliceous sediments (Jennings et al., 2006). *E. excavatum* and *C. reniforme* occur
403 together in glacial marine settings (Hald and Korsun, 1997). *C. reniforme* is also
404 considered to represent chilled Atlantic Water (Slubowska et al., 2005) [and is found in](#)
405 [areas of relatively high, stable salinities \(Polyak et al., 2002\)](#). *E. excavatum* is an
406 opportunistic species that thrives in unstable environmental conditions influenced by
407 rapid sedimentation and fluctuating salinities from turbid meltwater plumes (Hald and
408 Korsun, 1997). The agglutinated species, *Spiroplectammina biformis*, which occurs
409 mainly in the lower lithofacies unit is found in arctic fjords with strong meltwater signal
410 (Jennings and Helgadottir, 1994; Schaffer and Cole, 1986).

411 Several species indicative of marine productivity associated with nutrient rich
412 Atlantic Water occur in both the lower and upper lithofacies unit: *Melonis barleeanus*,
413 *Buccella frigida*, *Nonionella turgida* and *Nonionellina labradorica*. *Islandiella norcrossi*
414 and *I. helenae* both are arctic species, but *I. helenae* is associated with sea-ice edge
415 productivity while *I. norcrossi* reflects chilled Atlantic Water of normal marine salinity
416 [\(Polyak et al., 2002; Wollenburg et al., 2004; Lloyd, 2006\)](#). *I. norcrossi* is a common
417 calcareous species on the west Greenland shelf associated with Atlantic Water in the
418 West Greenland Current (e.g. Lloyd, 2006; Perner et al., 2012).

419 Near the top of the lower unit (16.5 cal ka BP), and continuing into the base of the
420 overlying biosiliceous mud, several species associated with marine productivity and
421 nutrient rich Atlantic Water spike to high percentages. These include *N. turgida*, *M.*

422 *barleeanus*, *B. frigida*, *I. norcrossi* and very low percentage of *Pullenia bulloides*.
423 Current indicator species, *Cibicides lobatulus* also increases at this boundary. The central
424 part of the [diatom-rich](#) mud is barren of calcareous foraminifers and is characterized by
425 low faunal abundances dominated by agglutinated foraminiferal species (e.g. *Textularia*
426 *earlandi*), suggesting that dissolution of carbonate likely overprinted the assemblages.
427 The upper part of the [diatom-rich](#) mud shows a return of several of the marine
428 productivity species along with increased percentages of *P. bulloides*, a chilled Atlantic
429 water species, that is common on the SE Greenland and Northern Iceland shelves under
430 conditions of strong Irminger Current Atlantic water inflow (Eiríksson et al., 2000;
431 Jennings et al., 2011b).

432 Above the [diatom-rich](#) mud, the percentages of *N. labradorica* and *I. norcrossi*
433 increase, and *S. feytingi* continues with high percentages. The chilled Atlantic Water
434 species, *Cassidulina neoteretis*, is abundant at the top of the dated section along with *I.*
435 *norcrossi*, consistent with intermediate Atlantic Water and less prominent glacial
436 meltwater influence (Jennings and Helgadottir, 1993). The gap in foraminifers between
437 12 and 13.9 cal ka BP is likely a consequence of carbonate dissolution as other cores
438 from the central West Greenland margin, but in slightly shallower water (JR175-VC29;
439 Fig. 1) have *C. neoteretis* continuously between 14 and 11 cal ka BP (Jennings et al., [in](#)
440 [revision2017](#)).

441 4.2.3 Biomarkers

442 Further evidence of marine productivity and sea ice comes from the algal biomarkers
443 brassicasterol and IP₂₅ (Fig. 5). In general, the presence of IP₂₅ indicates release from
444 melting seasonal sea ice (Fahl and Stein, 2012; Belt et al., 2013), while the absence of

445 IP₂₅ is consistent with intervals of thick perennial sea ice cover or no ice cover at all (Fahl
446 and Stein, 2012). Brassicasterol implies productivity in open-water conditions, but it also
447 can come from melting sea ice (Belt et al., 2013). In addition, the occurrence of polynyas
448 has been given as a possible reason for presence of IP₂₅ and brassicasterol under
449 otherwise heavy ice conditions, even in the central Arctic Ocean (Xiao et al., 2013).

450 In the lower, high CT lithofacies unit of 12PC, brassicasterol and IP₂₅ are present
451 in low abundances from 26 to 22 ka ($\Delta R=140$ yrs), coinciding with low foraminiferal
452 abundances (Fig. 5). Between 22 and 20 ka, brassicasterol rises but IP₂₅ is low to absent.
453 Foraminiferal abundances rise in this interval and the benthic fauna is characterized by
454 productivity species (*B. frigida*, *I. helenae*, *M. barleeanus* and *N. labradorica*). An
455 overall rise in IP₂₅ and a large peak in brassicasterol occur at 19.5 ka, and continue with
456 moderate values until another rise in brassicasterol values within the [biosiliceous-diatom-](#)
457 [rich](#) mud unit (16.2 to 15.1 cal ka BP). Both IP₂₅ and brassicasterol continue to rise after
458 15.1 cal ka BP, but IP₂₅ in particular rises to values unprecedented in the core after 14.3
459 cal ka BP.

460 This pattern of presence of IP₂₅ and brassicasterol in the lower lithofacies unit
461 argues for seasonal sea ice and some open water, although the generally low
462 concentrations suggest that these were both likely less than in the upper unit - probably
463 due to more extensive ice cover and only periodic opening - possibly as leads or
464 polynyas. As the final increase in IP₂₅ beginning at 16.2 ka is accompanied by rising,
465 high brassicasterol it likely points to development of a marginal ice zone where there is
466 increased marine productivity with probably more seasonal sea ice presence than before.

467

468 **5. Discussion**

469 5.1 Did an LGM Ice Shelf cover Baffin Bay?

470 There has been limited research on the LGM within Baffin Bay, which explains
471 how the Baffin Bay ice shelf concept has remained untested. Radiocarbon dates on
472 planktic foraminifers indicate that other cores besides 12PC have planktic fauna in the
473 LGM. Andrews et al (1998) obtained a pair of AMS ^{14}C dates from abundant planktic
474 foraminifera in southern Baffin Bay core HU77029-017PC ($17,990 \pm 110$, and $17,930 \pm$
475 210 ^{14}C yrs; Andrews et al., 1998) (Fig. 1). These ^{14}C ages calibrate to the LGM (~ 21 ka
476 BP; $\Delta R=140$ years). A ^{14}C date on planktic foraminifers from core HE006-4-2PC
477 ($21,440 \pm 140$ ^{14}C yrs) on the northern side of the Uummannaq TMF (Fig. 1) calibrates to
478 ~ 25 ka BP ($\Delta R=140$ years) (Ó Cofaigh et al., 2013a). In the LGM interval of 12PC (1130
479 cm to at least 690 cm) when the modeled Baffin Bay ice shelf would be in place, there
480 are multiple lines of evidence for biological activity, including bioturbation, algal
481 biomarkers and benthic and planktic foraminifers (Figs. 3 - 6). These findings are
482 consistent with perennial sea-ice cover with some open water in the form of leads or
483 polynyas on the eastern side of Baffin Bay. Full ice-shelf cover from an ice shelf
484 extending from the Hudson Strait ice stream and grounding on Davis Strait all the way to
485 Greenland (Alvarez-Solas et al., 2010; 2011; Marcott et al., 2011) would not allow the
486 surface productivity (e.g. algal biomarkers, planktic forams) in Baffin Bay that would be
487 needed to feed the benthic organisms that are evident (bioturbation and benthic
488 foraminifers). On this basis we reject the modeling result of a full Baffin Bay ice shelf.
489 While life has been observed under modern ice shelves in Antarctica, it is dependent on
490 strong ocean inflow to the sub ice-shelf cavity from outside the ice shelf (Post et al.,

491 2014). In the case of the Baffin Bay ice shelf cover as it is modeled, it would be sealed
492 from the Labrador Sea marine advection and food supply.

493 The idea of the Davis Strait grounded ice shelf sprang in part from efforts to test a
494 mechanism for Heinrich Event 1 (H1), in which subsurface warming reconstructed in the
495 N. Atlantic in response to reduced Atlantic meridional overturning circulation (AMOC)
496 during HS1 (McManus et al., 2004) weakens a buttressing ice shelf fronting the Hudson
497 Strait ice stream and produces a Heinrich event (Álvarez-Solas et al., 2010; 2011;
498 Marcott et al., 2011). Hulbe et al. (2004) modified their original 1997 Labrador Sea ice
499 shelf idea to support instead fringing ice shelves along the coasts in Eastern Canada that
500 were proposed to have met their demise through a process of meltwater infilling of
501 surface crevasses. The existence of this type of ice shelf and H-event process has been
502 contested (Alley et al., 2005), but it is more consistent with the 12PC data than the
503 original idea of an ice shelf grounding on Davis Strait (Hulbe et al., 1997).

504 *5.2 Heinrich Stadial Environments*

505 The data in 12PC allow examination of the environmental response in Baffin Bay
506 to the transition from LGM to HS1, and the response in Baffin Bay to the large ice
507 discharge from Hudson Strait during H1 which occurred when subsurface ocean heat was
508 at a maximum and AMOC at a minimum (Marcott et al., 2011). Locating the LGM/HS1
509 transition and H1 in 12PC is made difficult by the uncertainties in the magnitude of the
510 local marine reservoir age through time (Fig. 3F) (Stern and Lisiecki, 2013). The
511 accepted timing of H1 calving event is 16.8 ka BP (Hemming, 2004), although it may be
512 closer to 16 ka BP based on the timing of the peak of IRD in the North Atlantic IRD
513 stack during HS1 (Stern and Lisiecki, 2013). If we apply the ΔR [envelope](#)

514 approach using data from Stern and Lisiecki (2013) to the mean value of the best 2
515 constraining radiocarbon ages from the base of DC1 (=H1) in cores HU75009-IV-055PC
516 and HU87033-009 LCF (Fig. 1; Andrews et al., 1994; Jennings et al., 1996), from the
517 Labrador Sea, we obtain a range of ages for the event that spans HS1 (Table 1). The ΔR
518 that matches best the H1 16.8 ka age determined by Hemming (2004) is the lower ΔR
519 from Stern and Lisiecki (2013) (Table 1). On this basis, we chose to use the Lower ΔR to
520 determine where HS1 lies in the 12PC record. Lower ΔR places the base of HS1 [\(18 ka](#)
521 [BP\)](#) at 610 cm and its end [\(14.7 ka BP\)](#) at 395cm, right at the end of the [diatomaceous](#)
522 [diatom-rich](#) mud unit and before the initiation of calving retreat (Fig. 3F and 7). Lower
523 ΔR also puts the calving retreat and the timing of the west Greenland DC event
524 [\(=BBDC1; Jackson et al., 2017\) \(Fig. 3\)](#) in the Bølling/Allerød interstadial (Fig. 7). The
525 age model calculated with an invariant $\Delta R=140$ years places the [lithofacies](#) transition
526 [which represents the grounding line retreat from the west Greenland shelf edge](#) at 16.2
527 cal ka BP, within HS1 (Jennings et al., [in-revision2017](#)), but places the end of HS1 after
528 the initiation of GIS calving retreat.

529 Figure 7 illustrates how key proxy data map into the Heinrich Stadial interval
530 defined by evidence of sluggish AMOC (McManus et al., 2004) [using the lower \$\Delta R\$ of](#)
531 [Stern and Lisiecki \(2013\)](#). In the Labrador Sea HS1 is an interval of anomalously warm
532 bottom waters (Marcott et al., 2011) within which H1 occurred (Fig. 7). We would
533 expect this massive freshwater (meltwater and icebergs) outflow from collapse of the
534 Hudson Strait ice stream (Andrews and Tedesco, 1992; Hesse and Khodabakhsh, 2016)
535 to perturb environments in Baffin Bay or initiate a transition to different
536 paleoceanographic conditions.

537 The transition to lighter $\delta^{18}\text{O}$ values and a shift to very high percentages of *S.*
538 *feylingi* coincide with HS1 (Fig. 7). This signal is also seen in nearby core JR175-VC29
539 (Fig. 1), from 900 m water depth (Jennings et al., [in-revision2017](#)) and is associated in
540 both 12PC and VC29 with deposition of ~~diatomaceous bioturbated~~ diatom-rich mud with
541 rare IRD; a fine-grained unit of similar age is observed in core GeoTü SL-170 (Jackson et
542 al., 2017) slightly north of VC29. This diatom-rich mud interval has been interpreted by
543 Jennings et al. ([in-revision2017](#)) to ~~indicate protection of the~~ indicate exclusion of coarse
544 sediment delivery to the Disko TMF by retention of a fringing ice shelf Disko Trough
545 Mouth fan from coarse sediments released at the grounding line sediments by retreat of
546 the grounding line but retention of a fringing ice shelf after initial grounding line retreat.
547 Overall, brassicasterol abundances are low in HS1. A period of high productivity of
548 benthic forams indicative of nutrient rich Atlantic water at the subsurface (Fig. 5)
549 (indicated on Fig. 7 by red stars and the low percentages of the benthic foraminiferal
550 species, *S. feylingi*) coincides with the initial GIS retreat from the shelf edge as indicated
551 in the CT# profile (Jennings et al., [in-revision2017](#)). Subsequent interstadial conditions
552 are marked by rising marine productivity, renewed subsurface Atlantic Water influence,
553 and renewed retreat of the GIS, followed by development of consistent seasonal sea ice
554 and release/melting of detrital carbonate bearing ice bergs from ice margins of northern
555 Baffin Bay termed a west Greenland DC event by (Jennings et al., [in-revision2017](#)) that
556 has been shown to be correlative to BBDC1 (Simon et al. (2016) by Jackson et al. (2017).

557

558 **6. Conclusions**

559 1. Based on the data presented we reject the hypothesis that Baffin Bay was covered by a
560 full ice shelf during the LGM. We conclude ~~instead that rather than being completely~~
561 ~~covered by an ice shelf, that~~ Baffin Bay was perennially sea-ice covered ~~in the LGM with~~
562 nutrient rich, relatively warm Atlantic water present at depth through the LGM. Evidence
563 of marine productivity suggests that there were openings in the sea-ice cover as leads and
564 polynyas to support marine productivity. Concurrently, sediment-laden, glacial-meltwater
565 and turbidity currents were released from the GIS, grounded at the shelf edge, but IRD
566 was rare suggesting the ice front was protected by a fringing ice shelf and/or the
567 perennial sea-ice cover.

568 2. Reduced ventilation and productivity, coincident with a cold surface lid of meltwater
569 was established in HS1. After Heinrich Event 1, but within the Heinrich stadial, an
570 interval of increased productivity and Atlantic Water is associated with the retreat of the
571 GIS grounding line from the shelf edge.

572 3. The implication for Heinrich Events and Ocean warming/Ice Shelf hypothesis is that
573 perennial sea-ice cover and/or fringing ice shelves may be sufficient to explain the heat
574 retention and back-pressure proposed to explain the dynamics that produce Heinrich
575 Events.

576

577 **7. Acknowledgements**

578 Funding for this research was provided by the US National Science Foundation grant
579 ARC1203492 and the UK Natural Environment Research Council grant NE/D001951/1.
580 We thank the captain, crew and scientists aboard the 2008 CSS Hudson cruise HU2008-
581 029 for acquisition of core 2009029-12PC. We gratefully acknowledge the microscope

582 and x-ray diffraction research by undergraduate research assistants, Brian Shreve,
583 Jennifer Kelly, Matthew Reed, and Matthew Glasset. [We thank Quentin Simon and one](#)
584 [anonymous reviewer for helpful critique of the manuscript.](#)

585

586 **8. Figure Captions**

587 Figure 1. Bathymetric map centered on Baffin Bay (BB) showing the location of core
588 HU2008029-12PC (12PC) and other cores mentioned in the text, the distribution of
589 Paleozoic carbonate bedrock, mapped ice margin positions in northern Baffin Bay (Li et
590 al., 2011) and central west Greenland (Ó Cofaigh et al., 2013a) and major ice streams.
591 UIS = Uummanaq ice stream; DIS = Disko ice stream; SSIS = Smith Sound ice stream;
592 LSIS = Lancaster Sound ice stream. Northward flowing West Greenland Current (WGC)
593 is shown [as](#) the thin red line and the southward flowing Baffin Current (BC) is shown as
594 a thin blue line. The position of the acoustic profile in Figure 2 is shown [as](#) a black line.
595 HU2008029-016PC=16; HE006-4-2PC=2; JR175-VC29=29; HU77029-017PC=17;
596 HU75009-IV-055PC=55 and HU87033-009 LCF=9. [Inset plot shows the salinity and](#)
597 [temperature against water depth at from the same location as 2008029-12PC.](#)
598 [ASW=Arctic Surface Water; WGIW=West Greenland Intermediate Water; DBBW=Deep](#)
599 [Baffin Bay Water.](#)

600

601 Figure 2. [A.](#) 3.5 kHz sub-bottom profile over the site of 2008029-12PC demonstrating
602 the acoustically-stratified character of the seabed in the area. [B.](#) [A zoom in map of the 3.5](#)
603 [kKz sub-bottom profile and the core location shown in Figure 1. The bathymetry is from](#)
604 [GEBCO.](#)

605

606 Figure 3. Lithological proxies and age control for 2008029-12PC. A is the CT image
607 against depth in the core. Black bars along depth axis show the locations of CT images
608 shown in Figure 4. 'V' denotes locations of vertical burrows. B. IRD counts (>2mm
609 clasts) from CT scan in 2 cm increments. C. CT number, a measure of density derived
610 from the CT image. D. Magnetic Susceptibility measure by multi sensor track (MST). E.
611 Weight percentage of >63 μm sand fraction from foraminiferal samples. F. Two-source
612 provenance of minerals: Northern Baffin Bay (NBB, brown) vs. the local source, central
613 west Greenland (green). F. Depth-Age model in pink ($\Delta R=140\pm 30$ yrs) showing 1σ and
614 2σ uncertainties of the model. Excluded from the model are benthic foraminiferal ages
615 (green distributions) and outliers at 1 meter. Age ~~envelope~~ envelope for other potential ΔR
616 calibrations are shown by blue ($\Delta R=0$); Red, green, orange = lower, mean, and upper ΔR
617 values from Stern and Lisiecki, (2013). Climate units are along the age scale.

618

619 Figure 4. Examples of lithofacies and bioturbation types from 2008029-12PC CT scans.

620 [See Figure 3 for locations of these examples on the CT image of the core.](#)

621

622 Figure 5. Biological proxies from 12PC [compared with CT# plot to assist with](#)
623 [comparison to depth on depth in Figure 3. A. CT#; B. sea ice biomarker, IP₂₅; C. marine](#)
624 [productivity biomarker, brassicasterol; D. Benthic \(blue\) and planktic \(red\) forams per](#)
625 [gram of dry sediment; E. \$\delta^{18}\text{O}\$ of planktic foraminifer, *N. pachyderma*, blue; F. \$\delta^{13}\text{C}\$ of *N.*](#)
626 [pachyderma, green.](#)

627 Figure 6. Benthic foraminiferal species in 12PC. Green represent marine productivity
628 species; Red=Atlantic Water species; Blue = Arctic species; Light Blue; Glacial marine
629 species; [Orange=transformed \(cooler and slightly lower salinity\) Atlantic Water species.](#)

630

631 Figure 7. Comparison between Pa/Th record of AMOC (McManus et al., 2004) and the
632 timing of [Heinrich Event 1 \(H1\)](#) to key paleoenvironmental proxies in 12PC. The HS1
633 interval (yellow box) is defined in the core with use of the Lower ΔR of Stern and
634 Lisiecki (2013) (Fig. 3f). Blue lines show where key events in the core map into the
635 climatic intervals [with use of the Lower \$\Delta R\$ of Stern and Lisiecki \(2013\)](#). A. CT # from
636 12PC; B. Brassicasterol, 12PC; C. IP₂₅, 12PC; D. *Stainforthia feylingi*, 12PC; E. Oxygen
637 isotope ratios, 12PC; F. Pa/Th ratios (McManus et al., 2004).

638 **References Cited**

639

640 Aksu, A. E., 1985. Climatic and oceanographic changes over the past 400,000 years:
641 Evidence from deep-sea cores on Baffin Bay and David Strait. *In* Andrews, J. T. (ed.),
642 *Quaternary Environments: Eastern Canadian Arctic, Baffin Bay and Western*
643 *Greenland*. Boston: Allen and Unwin, 181-209.

644

645 Alley, R. B., Andrews, J. T., Barber, D. C., and Clark, P. U., 2005: Comment on
646 "Catastrophic ice shelf breakup as the source of Heinrich event icebergs" by C.L.
647 Hulbe et al. *Palaeoceanography*, 20: doi:10.1029/2004PA001086.

648

649 Álvarez-Solas, J., Charbit, S., Ritz, C., Paillard, D., Ramstein, G., and Dumas, C.: Links
650 between ocean temperature and iceberg discharge during Heinrich events, *Nature*
651 *Geoscience*, 3, 122–126, 2010

652

653 Álvarez-Solas, J., Montoya, M., Ritz, C., Ramstein, G., Charbit, S., Dumas, C.,
654 Nisancioglu, K., Dokken, T., Ganopolski, A., 2011. Heinrich event 1: an example of
655 dynamical ice-sheet reaction to ocean changes. *Climate of the Past* 7, 1297-1306.
656 doi:10.5194/cp-7-1297-2011.

657

658 Andrews, J.T., Eberl, D.D., 2011. Surface (sea floor) and near-surface (box cores)
659 sediment mineralogy in Baffin Bay as a key to sediment provenance and ice sheet
660 variations. *Can. J. Earth Sci.* 48 (9), 1307 - 1328. <http://dx.doi.org/10.1139/-11-021>.

661

662 Andrews, J.T., Eberl, D.D., 2012. Determination of sediment provenance by unmixing
663 the mineralogy of source-area sediments: The "SedUnMix" program. *Marine Geology*
664 291, 24-33.

665
666 Andrews, J.T., Erlenkeuser, H., Tedesco, K., Aksu, A., Jull, A.J.T., 1994. Late Quaternary
667 (Stage 2 and 3) Meltwater and Heinrich events, NW Labrador Sea. *Quaternary*
668 *Research* 41, 26-34.

669
670 Andrews, J.T., Gibb, O.T., Jennings, A.E., Simon, Q., 2014. Variations in the provenance
671 of sediment from ice sheets surrounding Baffin Bay during MIS 2 and 3 and export
672 to the Labrador Shelf Sea: site HU2008029-0008 Davis Strait. *Journal of Quaternary*
673 *Science* 29, 3-13.

674
675 Andrews, J. T., Kirby, M. E., Aksu, A., Barber, D. C., and Meese, D., 1998. Late
676 Quaternary Detrital Carbonate (DC-) events in Baffin Bay (67° - 74° N): Do they
677 correlate with and contribute to Heinrich Events in the North Atlantic? *Quaternary*
678 *Science Reviews*, 17: 1125-1137.

679
680 Andrews, J. T. and Tedesco, K., 1992: Detrital carbonate-rich sediments,
681 northwestern Labrador Sea: Implications for ice-sheet dynamics and iceberg rafting
682 (Heinrich) events in the North Atlantic. *Geology*, 20: 1087-1090.

683
684 Belt, S.T., Brown, T.A., Navarro Rodriguez, A., Cabedo Sanz, P., Tonkin, A., Ingle, R.,
685 2012. A reproducible method for the extraction, identification and quantification of
686 the Arctic sea ice proxy IP25 from marine sediments. *Analytical Methods* 4, 705-713.

687
688 Belt, S.T., Brown, T.A., Ringrose, A.E., Cabedo-Sanz, P., Mundy, C.J., Gosselin, M.,
689 Poulin, M., 2013. Quantitative measurement of the sea ice diatom biomarker IP25
690 and sterols in Arctic sea ice and underlying sediments: Further considerations for
691 palaeo sea ice reconstruction. *Organic Geochemistry* 62, 33-45.

692
693 Belt, S.T., Cabedo-Sanz, P., Smik, L., Navarro-Rodriguez, A., Berben, S.M., Knies, J.,
694 Husum, K., 2015. Identification of paleo Arctic winter sea ice limits and the marginal
695 ice zone: Optimised biomarker-based reconstructions of late Quaternary Arctic sea
696 ice. *Earth and Planetary Science Letters* 431, 127-139.

697
698 Blake, W., Jr. 1977. Glacial sculpture along the east-central coast of Ellesmere Island,
699 Arctic Archipelago. Current Research, Part C, Geological Survey of Canada, Paper 77-
700 1C, 107-115.

701
702 Briner, J. P., Miller, G. H., Davis, P. T., Bierman, P. R., and Caffee, M., 2003. Last Glacial
703 Maximum ice sheet dynamics in Arctic Canada inferred from young erratics perched
704 on ancient tors. *Quaternary Science Reviews*, 22: 437-444.

705

706 Brown, T.A., Belt, S.T., 2012. Closely linked sea ice–pelagic coupling in the Amundsen
707 Gulf revealed by the sea ice diatom biomarker IP25. *Journal of plankton research* 34,
708 647-654.

709

710 Buch E. 2000a. A monograph on the physical oceanography of the Greenland waters.
711 Danish Meteorological Institute Scientific Report, 00-12.

712

713 Buch E. 2000b. Air-sea-ice conditions off southwest Greenland, 1981–1997. *Journal*
714 *of Northwest Atlantic Fisheries Science* 26, 1–14.

715

716 Buizert, C., Gkinis, V., Severinghaus, J.P., He, F., Lecavalier, B.S., Kindler, P.,
717 Leuenberger, M., Carlson, A.E., Vinther, B., Masson-Delmotte, V., White, J.W.C., Liu, Z.,
718 Otto-Bliesner, B., Brook, E.J., 2014. Greenland temperature response to climate
719 forcing during the last deglaciation. *Science* 345, 1177-1180. DOI:
720 10.1126/science.1254961

721

722 Campbell, D C, de Vernal, A., 2009. CCGS Hudson Expedition 2008029: marine
723 geology and paleoceanography of Baffin Bay and adjacent areas, Nain, NL to Halifax,
724 NS, August 28-September 23. Geological Survey of Canada, Open File 5989, 2009,
725 212 pages; 1 DVD, doi:10.4095/261330

726

727 Clark, P.U., Dyke, A.S., Shakun, D., Carlson, A.E., Clark, J., Wohlfarth, B., Mitrovica, J.X.,
728 Hostetler, S.W., McCabe, A.M., 2009. The Last Glacial Maximum. *Science* 325, 710-
729 714.

730

731 Dahl-Jensen, D. and al., e., 1998: Past Temperatures Directly from the Greenland Ice
732 Sheet. *Science*, 282: 268-271.

733

734 Darling, K. F., Kucera, M., Kroon, D., Wade, C.M., 2006. A resolution for the coiling
735 direction paradox in *Neogloboquadrina pachyderma*. *Paleoceanography* 21,
736 PA2011, doi:10.1029/2005PA001189.

737

738 de Vernal, A., Bilodeau, G., Hillair -Marcel, C., Kassou, N., 1992. Quantitative
739 assessment of carbonate dissolution in marine sediments from foraminifer linings
740 vs. shell ratios: example from Davis Strait, NW North Atlantic, *Geology*, 20: 527-530.

741

742 Domack, E.W., Harris, P.T., 1998. A new depositional model for ice shelves, based
743 upon sediment cores from the Ross Sea and the Mac. Roberson shelf, Antarctica.
744 *Annals of Glaciology* 27, 281-284.

745

746 Dowdeswell, J.A., Hogan, K.A., Ó Cofaigh, C., Fugelli, E.M.G., Evans, J., Noormets, R.,
747 2014. Late Quaternary ice flow in a West Greenland fjord and cross-shelf trough
748 system: submarine landforms from Rink Isbrae to Uummannaq shelf and slope.
749 *Quat. Sci. Rev.* 92, 292-309. <http://dx.doi.org/10.1016/j.quascirev.2013.09.007>.

750

751 Dyke, A. S., Andrews, J. T., Clark, P. U., England, J. H., Miller, G. H., Shaw, J., and
752 Veillette, J. J., 2002: The Laurentide and Innuitian ice sheets during the Last Glacial
753 Maximum. *Quaternary Science Reviews*, 21, 9-31.
754
755 Eberl, D.D., 2003. User guide to RockJock: A program for determining quantitative
756 mineralogy from X-ray diffraction data. United States Geological Survey, Open File
757 Report 03-78, 40 pp, Washington, DC.
758
759 Eiríksson, J., Knudsen, K.L., Hafliðason, H., Henriksen, P., 2000. Late-glacial and
760 Holocene palaeoceanography of the North Icelandic shelf. *Journal of Quaternary
761 Science* 15, 23-42.
762
763 England, J. 1999. Coalescent Greenland and Innuitian ice during the Last Glacial
764 Maximum: Revising the Quaternary of the Canadian High Arctic. *Quaternary Science
765 Reviews* 18, 421–426, [http://dx.doi.org/10.1016/S0277-3791\(98\)00070-5](http://dx.doi.org/10.1016/S0277-3791(98)00070-5).
766
767 England, J., Atkinson, N., Bednarski, J., Dyke, A.S., Hodgson, D.A., Ó Cofaigh, C. 2006.
768 The Innuitian Ice Sheet: configuration, dynamics and chronology. *Quaternary
769 Science Reviews* 25, 689-703.
770
771 Fahl, K., Stein, R., 2012. Modern seasonal variability and deglacial/Holocene change
772 of central Arctic Ocean sea ice cover: New insights from biomarker proxy records.
773 *Earth and Planetary Science Letters* 351–352, 123–133.
774
775 Grobe, H., 1987. A simple method for the determination of ice-rafted debris in
776 sediment cores. *Polarforschung* 57 (3), 123-126.
777
778 Hald, M., Korsun, S. 1997. Distribution of modern benthic foraminifera from fjords of
779 Svalbard, European Arctic. *Journal of Foraminiferal Research* 27, 101–122.
780
781 Hemming, S.R., 2004. Heinrich events: massive late Pleistocene detritus layers of the
782 North Atlantic and their global climate imprint. *Rev. Geophys.* 42, RG1005.
783
784 Hesse, R., Khodabakhsh, S. 2016. Anatomy of Labrador Sea Heinrich layers. *Marine
785 Geology* 380, 44-86. <http://dx.doi.org/10.1016/j.margeo.2016.05.019>
786
787 Hesse, R., Khodabakhsh, S., Klauke, I., Ryan, WBF., 1997. Asymmetrical turbid
788 surface-plume deposition near ice-outlets of the Pleistocene Laurentide ice sheet in
789 the Labrador Sea. *Geo-Marine Letters*, 17, 179-187.
790
791 Hillaire-Marcel, C., de Vernal, A., 2008. Stable isotope clue to episodic sea-ice
792 formation in the glacial North Atlantic. *Earth and Planetary Science Letters*, 268,
793 143-150.
794

795 Hillaire-Marcel, C., de Vernal, A., Aksu, A.E., Macko, S., 1989. High-resolution
796 isotopic and micropaleontological studies of upper Pleistocene sediments at ODP
797 Site 645, Baffin Bay, Proceedings of the Ocean Drilling Program, 105B: 599-616.
798
799 Hofmann, J.C., Knutz, P.C., Nielsen, T., Kuijpers, A., 2016. Seismic architecture and
800 evolution of the Disko Bay trough-mouth fan, central West Greenland margin,
801 *Quaternary Science Reviews*, <http://dx.doi.org/10.1016/j.quascirev.2016.05.019>
802
803 Holland, D.M., Thomas, R.H., de Young, B., Ribergaard, M.H., Lyberth, B., 2008.
804 Acceleration of Jakobshavn Isbræ triggered by warm subsurface ocean waters.
805 *Nature Geoscience* 1 (10), 659e664. <http://dx.doi.org/10.1038/ngeo316>.
806
807 Hulbe, C.L., 1997. An ice shelf mechanism for Heinrich layer production,
808 *Paleoceanography* 12, 711 –717.
809
810 Hulbe, C. L., MacAyeal, D. R., Denton, G. H., Kleman, J., and Lowell, T. V., 2004:
811 Catastrophic ice shelf breakup as the source for Heinrich event icebergs.
812 *Palaeoceanography*, 19: 1 of 15, doi.10.1029/2003:PA000890, 002004.
813
814 [Jackson, R., Carlson, A.E., Hillaire-Marcel, C., Wacker, L., Vogt, C., Kucera, M., 2017.](http://dx.doi.org/10.1016/j.quascirev.2017.03.020)
815 [Asynchronous instability of the North American-Arctic and Greenland ice sheets](http://dx.doi.org/10.1016/j.quascirev.2017.03.020)
816 [during the last deglaciation. *Quaternary Science Reviews* 164, 140-153.](http://dx.doi.org/10.1016/j.quascirev.2017.03.020)
817 [http://dx.doi.org/10.1016/j.quascirev.2017.03.020.](http://dx.doi.org/10.1016/j.quascirev.2017.03.020)
818
819 Jennings, A.E., Andrews, J.T., Ó Cofaigh, C., St. Onge, G., Sheldon, C., Belt, S.T., Cabedo-
820 Sanz, P., Hillaire-Marcel, C. ~~in revision~~ 2017. Ocean forcing of Ice Sheet Retreat in
821 Central West Greenland from LGM through Deglaciation. *Earth and Planetary*
822 *Science Letters* [472, 1-13](https://doi.org/10.1016/j.epsl.2017.03.020).
823
824 Jennings, A.E., Andrews, J.T., Wilson, L., 2011b. Holocene Environmental Evolution of
825 the SE Greenland Shelf North and South of the Denmark Strait: Irminger and East
826 Greenland Current Interactions. *Quaternary Science Reviews* 30: 980-998.
827
828 Jennings, A.E., Hald, M., Smith, L.M., and Andrews, J.T., 2006. Freshwater forcing
829 from the Greenland Ice Sheet during the Younger Dryas: Evidence from
830 southeastern Greenland shelf cores: *Quaternary Science Reviews* 25, 282–298,
831 doi:10.1016/j.quascirev.2005.04.006.
832
833 Jennings, A.E., Helgadottir, G., 1994. Foraminiferal assemblages from the fjords and
834 shelf of eastern Greenland. *J. Foraminifer. Res.* 24 (2), 123e144.
835 <http://dx.doi.org/10.2113/gsjfr.24.2.123>.
836
837 Jennings, A.E., Sheldon, C., Cronin, T.M., Francus, F., Stoner, J., Andrews, J., 2011a. The
838 Holocene history of Nares Strait, transition from glacial bay to Arctic-Atlantic
839 throughflow. *Oceanography* 24, no. 3, 26-41.
840

841 Jennings, A. E., Tedesco, K. A., Andrews, J. T., and Kirby, M. E., 1996. Shelf erosion and
842 glacial ice proximity in the Labrador Sea during and after Heinrich events (H-3 or 4
843 to H-0) as shown by foraminifera. *In* Andrews, J. T., Austin, W. E. N., Bergsten, H., and
844 Jennings, A. E. (eds.), *Late Quaternary Palaeoceanography of the North Atlantic*
845 *Margins*. Geological Society Special Publications, 29-49.

846

847 Jennings, A.E., Walton, M.E., Cofaigh, C._O., Kilfeather, A., Andrews, J.T., Ortiz, J.D., et
848 al., 2014. Paleoenvironments during Younger Dryas-early Holocene retreat of the
849 Greenland ice sheet from outer Disko Trough, central west Greenland. *J. Quat. Sci.* 29
850 (1), 27e40. <http://dx.doi.org/10.1002/jqs.2652>.

851

852 Kaufman, D.S., Williams, K.M. (compilers), 1992. Radiocarbon Date List VII: Baffin
853 Island, N.W.T., Canada. INSTAAR Occasional Paper 48. Institute of Arctic and Alpine
854 Research, University of Colorado, Boulder.

855

856 Knutz, P. C., M.-A. Sicre, H. Ebbesen, S. Christiansen, and A. Kuijpers, 2011. Multiple-
857 stage deglacial retreat of the southern Greenland Ice Sheet linked with Irminger
858 Current warm water transport, *Paleoceanography* 26, PA3204,
859 doi:10.1029/2010PA002053.

860

861 Li, G., Piper, D. J. W., and Campbell, D. C., 2011: The Quaternary Lancaster Sound
862 trough-mouth fan, NW Baffin Bay. *Journal of Quaternary Science*, 26: 511-522.

863 Lloyd, J. M. 2006. Modern distribution of benthic foraminifera from Disko Bugt, West
864 Greenland. *Journal of Foraminiferal Research* 36, 315-331.

865

866 Lloyd, J.M., Moros, M., Perner, K., Telford, R.J., Kuijpers, A., Jansen, E., et al., 2011.A
867 100 yr record of ocean temperature control on the stability of JakobshavnIsbrae,
868 West Greenland. *Geology* 39 (9), 867-870. <http://dx.doi.org/10.1130/G32076.1>.

869

870 Löwemark, L., O'Regan, M., Hanebuth, T.J.J., Jakobsson, M., 2012. Late Quaternary
871 spatial and temporal variability in Arctic deep-sea bioturbation and its relation to
872 Mn cycles. *Palaeogeography, Palaeoclimatology, Palaeoecology* 365-366, 192-208.

873

874 Lucci, RG and Rebesco, M., 2007. Glacial contourites on the Antarctic Peninsula
875 margin: insight for palaeoenvironmental and palaeoclimatic conditions. Geological
876 Society, London, Special Publications, 276: 111-127.

877

878 Marcott et al., 2011. Ice-shelf collapse from subsurface warming as a trigger for
879 Heinrich Events. *PNAS* 108. No. 33 p. 13415-13419

880

881 McManus, J.F., Francois, R., Gherardi, J.-M., Keigwin, L.D., Brown-Leger, S., 2004.
882 Collapse and rapid resumption of the Atlantic meridional circulation linked to
883 deglacial climate change. *Nature* 428, 834-837.

884

885 Münchow A., Falkner, A. Melling, H., 2015. Baffin Island and West Greenland Current
886 Systems in northern Baffin Bay. *Progress in Oceanography* 132, 305-317

887
888 Ó Cofaigh C., Andrews JT, Jennings AE, Dowdeswell JA, Hogan KA, Kilfeather AA, et
889 al. (2013a) Glacimarine lithofacies, provenance and depositional processes on a West
890 Greenland trough-mouth fan. *Journal of Quaternary Science* 28. Available at:
891 <http://dx.doi.org/10.1002/jqs.2569>: doi:10.1002/jqs.2569.
892
893 Ó Cofaigh C, Dowdeswell J.A., 2001. Laminated sediments in glacimarine environments:
894 diagnostic criteria for their interpretation. *Quaternary Science Reviews* 20, 1411-1436.
895
896 Ó Cofaigh C., Dowdeswell J.A., Jennings A.E., Hogan K.A., Kilfeather A., Hiemstra
897 J.F., et al. (2013b) An extensive and dynamic ice sheet on the West Greenland shelf
898 during the last glacial cycle. *Geology* 41(2): 219–222: doi:10.1130/G33759.1.
899
900 Nørgaard-Pedersen, N., Spielhagen, R.F., Erlenkeuser, H., Grootes, P.M., Heinemeier,
901 J., Knies, J. , 2003. Arctic Ocean during the Last Glacial Maximum: Atlantic and polar
902 domains of surface water mass distribution and ice cover. *Paleoceanography* 18,
903 doi:10.1029/2002PA000781, 2003.
904
905 Perner, K., Moros, M., Jennings, A., Lloyd, J.M., Knudsen, K.L., 2012. Holocene
906 palaeoceanographic evolution off West Greenland. *The Holocene* 23, 374-387.
907
908 Piénkowski, A.J., England, J.H., Furze, M.F.A., Marret, F., Eynaud, F., Vilks, G., Maclean,
909 B., Blasco, S., Scourse, J.D., 2012. The deglacial to postglacial marine environments of
910 SEBarrow Strait, Canadian Arctic Archipelago. *Boreas* 41 (2), 141-179.
911 <http://dx.doi.org/10.1111/j.1502-3885.2011.00227.x>.
912
913 [Polyak, L., Korsun, S., Febo, L.A., Stanovoy, V., Khusid, T., Hald, M., Paulsen, B.E.,](#)
914 [Lubinski, D.J., 2002. Benthic foraminiferal assemblages from the southern Kara Sea,](#)
915 [a river influenced Arctic marine environment. *Journal Foraminiferal Research* 32,](#)
916 [252–273.](#)
917
918 Post, A.L., Galton-Fenzi, B.K., Riddle, M.J., Herraiz-Borreguero, L., O'Brien, P.E.,
919 Hemer, M.A., McMinn, A., Rasch, D., Craven, M., 2014. Modern sedimentation,
920 circulation and life beneath the Amery Ice Shelf, East Antarctica. *Continental Shelf*
921 *Research* 74. 77-87.
922
923 Quillmann, U., Andrews, J. T., and Jennings, A. E., 2009: *Radiocarbon Date List XI:*
924 *East Greenland shelf, West Greenland Shelf, Labrador Sea, Baffin Island shelf, Baffin*
925 *Bay, Nares Strait, and Southwest to Northwest Icelandic shelf.* Occasional Paper No.
926 59, INSTAAR, University of Colorado, Boulder, Boulder.
927
928 Ramsey, C.B. and Lee, S., 2013. Recent and planned developments of the program
929 OxCal. *Radiocarbon* 55, 720-730.
930

931 Reeh, N., Thomsen, H. H., Higgins, A. K., and Weidick, A., 2001: Sea ice and the
932 stability of north and northeast Greenland floating glaciers. *In* Jeffries, M. O. and
933 Eicken, H. (eds.), *Annals of Glaciology*, Vol 33, 474-480.
934

935 Reimer, P.J., Bard, E., Bayliss, A., Beck, J.W., Blackwell, P.G., Ramsey, C.B., Grootes,
936 P.M., Guilderson, T.P., Hafliðason, H., Hajdas, I., Hatté, C., Heaton, T.J., Hoffmann,
937 D.L., Hogg, A.G., Hughen, K.A., Kaiser, K.F., Kromer, B., Manning, S.W., Niu, M.,
938 Reimer, R.W., Richards, D.A., Scott, E.M., Southon, J.R., Staff, R.A., Turney, C.S.M.,
939 van der Plicht, J., 2013. IntCal13 and Marine13 radiocarbon age calibration curves 0-
940 50,000 years cal BP. *Radiocarbon* 55, 1869–1887. [http://dx.doi.org/10.2458/azu_js_rc.](http://dx.doi.org/10.2458/azu_js_rc.55.16947)
941 55.16947.
942

943 Reineck, H.E., Singh, I.B., 1980. *Depositional Sedimentary Environments*. Springer-
944 Verlag, NY.
945

946 Sarnthein, M., et al., Variations in Atlantic surface ocean paleoceanography, 50_–80_N:
947 A time-slice record of the last 30,000 years, *Paleoceanography*, 10(6), 1063– 1094, 1995.
948 Schafer, C.T., Cole, F.E., 1988. Environmental associations of Baffin Island fjord
949 agglutinated foraminifera. *Abh. Geol. Bundesanst*, 307.
950

951 Seidenkrantz, M.-S., 2013. Benthic foraminifera as palaeo sea-ice indicators in the
952 subarctic realm-examples from the Labrador Sea-Baffin Bay region. *Quaternary Science*
953 *Reviews* 79, 135-144. <http://dx.doi.org/10.1016/j.quascirev.2013.03.014>
954

955 Shaffer, G., Olsen, S.M., Bjerrum, C.J., 2004. Ocean subsurface warming as a
956 mechanism for coupling Dansgaard-Oeschger climate cycles and ice-rafting events.
957 *Geophysical Research Letters* 31, L24202. doi:10.1029/2004GL020968.
958

959 Sheldon, C., Jennings, A., Andrews, J.T., Ó Cofaigh, C., Hogan, K., Dowdeswell, J.A.,
960 Seidenkrantz, M.-S., 2016. Ice stream retreat following the LGM and onset of the west
961 Greenland current in Uummannaq Trough, west Greenland. *Quaternary Science Reviews*,
962 <http://dx.doi.org/10.1016/j.quascirev.2016.01.019>
963

964 Simon, Q., Hillaire-Marcel, C., St-Onge, G., Andrews, J.T., 2014. Northeastern
965 Laurentide, western Greenland and southern Inuitian ice stream dynamics during the last
966 glacial cycle. *Journal of Quaternary Science* 29(1): 14-26. DOI: 10.1002/jqs.2648
967

968 Simon Q, St-Onge G, Hillaire-Marcel C., 2012. Late Quaternary chronostratigraphic
969 framework of deep Baffin Bay glaciomarine sediments from high-resolution
970 paleomagnetic data. *Geochemistry, Geophysics, Geosystems* 13: Q0AO03. doi: 10.1029/
971 2012GC004272
972

973 [Simon, Q., Thouveny, N., Bourles, D.L., Nuttin, L., Hillaire-Marcel, C., St-Onge, G.,](#)
974 [2016. Authigenic ¹⁰Be/ ⁹Be ratios and ¹⁰Be-fluxes \(²³⁰Th_{xs}-normalized\) in central Baffin](#)
975 [Bay sediments during the last glacial cycle: Paleoenvironmental implications. *Quaternary*](#)
976 [Science Reviews](#) 140, 142-162.

977
978 Slabon, P., Dorschel, B., Jokat, W., Myklebust, R., Hebbeln, D., Gebhardt, C., 2016.
979 Greenland ice sheet retreat history in the northeast Baffin Bay based on high-resolution
980 bathymetry. *Quaternary Science Reviews* 154, 182-198.
981 <http://dx.doi.org/10.1016/j.quascirev.2016.10.022>
982
983 Slubowska, M.A., Koç, N., Rasmussen, T.L., Klitgaard-Kristensen, D., 2005. Changes in
984 the flow of Atlantic water into the Arctic Ocean since the last deglaciation: evidence from
985 the northern Svalbard continental margin, 80°N. *Paleoceanography* 20, PA4014.
986 doi:10.1029/2005PA001141.
987
988 Stern, J.V., Lisiecki, L.E. 2013. North Atlantic circulation and reservoir age changes over
989 the past 41,000 years. *Geophysical Research Letters* 40: 3693-3697.
990 doi:10.1002/grl.50679, 2013.
991
992 Straneo, F., Sutherland, D.A., Holland, D., Gladish, C., Hamilton, G.S., Johnson, H.L.,
993 Rignot, E., Xu, Y., Koppes, M., 2012. Characteristics of ocean waters reaching
994 Greenland's glaciers. *Annals of Glaciology* 53(60), 202-210.
995 doi:10.3189/2012AoG60A059
996
997 Tang, C.C.L., Ross, C.K., Yao, T., Petrie, B., DeTracey, B.M., Dunlap, E., 2004. The
998 circulation, water masses and sea-ice of Baffin Bay. *Progress in Oceanography* 63, 183–
999 228.
1000
1001 Wetzel, A., 1991. Ecologic interpretation of deep-sea trace fossil communities.
1002 *Palaeogeography, Palaeoclimatology, Palaeoecology* 85, 47-69.
1003
1004 Wollenburg, J.E., Knies, J., Mackensen, A., 2004. High-resolution paleoproductivity
1005 fluctuations during the past 24 kyr as indicated by benthic foraminifera in the
1006 marginal Arctic Ocean. *Palaeogeography, Palaeoclimatology, Palaeoecology* 204, 209–
1007 238.
1008
1009 Xiao, X., Fahl, K., Stein, R., 2013. Biomarker distributions in surface sediments from the
1010 Kara and Laptev seas (Arctic Ocean): indicators for organic-carbon sources and sea ice
1011 coverage. *Quaternary Science Reviews* 79, 40–52.
1012
1013 Zreda, M., England, F., Phillips, D., Elmore, and P. Sharma. 1999. Unblocking of the
1014 Nares Strait by Greenland and Ellesmere Ice-Sheet retreat 10,000 years ago. *Nature*
1015 398,139–142, <http://dx.doi.org/10.1038/18197>
1016

- Baffin Bay was not covered by an ice shelf in the LGM.
- Baffin Bay was perennially sea-ice covered through the LGM.
- LGM marine productivity promoted by leads and polynyas in perennial sea-ice cover.
- Heinrich stadial paleoenvironments vary and are associated with GIS retreat
- H1 Ice Shelf hypothesis rejected; no evidence for Baffin Bay full ice shelf.

1 **Baffin Bay Paleoenvironments in the LGM and HS1: Resolving the ice-shelf**
2 **question**

3
4 Anne E. Jennings^{1*}, John T. Andrews¹, Colm Ó Cofaigh², Guillaume St-Onge³, Simon
5 Belt⁴, Patricia Cabedo-Sanz⁴, Christof Pearce^{5,6}, Claude Hillaire-Marcel⁷, D. Calvin
6 Campbell⁸

7 ¹ INSTAAR University of Colorado, Campus Box 450, Boulder, CO 80309-0450 USA

8 ² Department of Geography, Durham University, South Road, Durham DH1 3LE, United
9 Kingdom

10 ³ Institut des sciences de la mer de Rimouski (ISMER) Université du Québec à Rimouski
11 and GEOTOP Rimouski, Québec, Canada S5L 3A1

12 ⁴ School of Geography, Earth and Environmental Sciences, University of Plymouth,
13 Plymouth PL4 8AA United Kingdom

14 ⁵ Department of Geological Sciences and Bolin Centre for Climate Research, Stockholm
15 University, Svante Arrhenius väg 8, SE-106 91 Stockholm, Sweden

16 ⁶ Department of Geoscience and Arctic Research Centre, Aarhus University, Hoegh
17 Guldbergs gade 2, 8000 Aarhus, Denmark

18 ⁷ Université du Québec a Montréal, Centre GEOTOP CP 8888, succ. Centre-Ville,
19 Montréal, Québec, Canada, H3C 3P8

20 ⁸ Geological Survey of Canada-Atlantic, Natural Resources Canada, Dartmouth Nova
21 Scotia

22 * anne.jennings@colorado.edu
23

24 Core HU2008029-12PC from the Disko trough mouth fan on the central West
25 Greenland continental slope is used to test whether an ice shelf covered Baffin Bay
26 during the Last Glacial Maximum (LGM) and at the onset of the deglaciation. We use
27 benthic and planktic foraminiferal assemblages, stable isotope analysis of planktic
28 forams, algal biomarkers, ice-rafted detritus (IRD), lithofacies characteristics
29 defined from CT scans, and quantitative mineralogy to reconstruct
30 paleoceanographic conditions, sediment processes and sediment provenance. The
31 chronology is based on radiocarbon dates on planktic foraminifers using a ΔR of 140
32 ± 30 ¹⁴C years, supplemented by the varying reservoir estimates of Stern and
33 Lisiecki (2013) that provide an envelope of potential ages. HU2008029-12PC is
34 bioturbated throughout. Sediments between the core base at 11.3 m and 4.6 m
35 (LGM through HS1) comprise thin turbidites, plumites and hemipelagic sediments
36 with Greenlandic provenance consistent with processes active at the Greenland Ice
37 Sheet margin grounded at or near the shelf edge. Abundance spikes of planktic
38 forams coincide with elevated abundance of benthic forams in assemblages
39 indicative of chilled Atlantic Water, meltwater and intermittent marine productivity.
40 IRD and IP₂₅ are rare in this interval, but brassicasterol, an indicator of marine
41 productivity reaches and sustains low levels during the LGM. These biological
42 characteristics are consistent with a sea-ice covered ocean experiencing periods of
43 more open water such as leads or polynyas in the sea ice cover, with chilled Atlantic
44 Water at depth, rather than full ice-shelf cover. They do not support the existence of
45 a full Baffin Bay ice shelf cover extending from grounded ice on the Davis Strait.
46 Initial ice retreat from the West Greenland margin is manifested by a pronounced
47 lithofacies shift to bioturbated, diatomaceous mud with rare IRD of Greenlandic
48 origin at 467 cm (16.2 cal ka BP; $\Delta R=140$ yrs) within HS1. A spike in foraminiferal
49 abundance and ocean warmth indicator benthic forams precedes the initial ice
50 retreat from the shelf edge. At the end of HS1, IP₂₅, brassicasterol and benthic

51 forams indicative of sea-ice edge productivity increase, indicating warming
52 interstadial conditions. Within the Bølling/Allerød interstadial a strong rise in IP₂₅
53 content and IRD spikes rich in detrital carbonate from northern Baffin Bay indicate
54 that northern Baffin Bay ice streams were retreating and provides evidence for
55 increased open water, advection of Atlantic Water in the West Greenland Current,
56 and formation of an IRD belt along the W. Greenland margin.

57
58 Keywords: Greenland Ice Sheet, Baffin Bay, paleoceanography, ice shelf,
59 foraminifera, Heinrich Stadial 1

60

61 **1. Introduction**

62

63 Last Glacial Maximum (LGM) climatic and oceanic conditions in Baffin Bay are
64 currently poorly known, but according to the temperature reconstructions from the
65 Greenland Ice Sheet borehole (Dahl-Jensen and al., 1998) and ice-core data (Buizert et
66 al., 2014), summit temperatures were ~20°C colder than present. Applying this
67 temperature difference down to sea level using the adiabatic lapse rate, suggests that the
68 annual temperature at the surface of Baffin Bay adjacent to Baffin Island would approach
69 -36°C. Such cold temperatures support the argument that cold-based ice covered the
70 forelands of eastern Baffin Island (Briner et al., 2003) with “Antarctic-like” conditions
71 across Baffin Bay, which would also suggest that Baffin Bay was covered in perennial
72 sea ice. At the LGM, confluent, Innuitian (IIS), Laurentide (LIS) and Greenland (GIS) ice
73 sheets (England et al., 2006) blocked the channels that connect Baffin Bay to the Arctic
74 Ocean (Dyke, 2002) and terminated in northern Baffin Bay as large ice streams (Li et al.,
75 2011; Blake, 1977). The Greenland ice sheet reached the continental shelf edge via large
76 ice streams off west Greenland (Ó Cofaigh et al., 2013a; Jennings et al., 2017; Slabon et
77 al., 2016; Sheldon et al., 2016; Dowdeswell et al., 2014), but the outer limits of the ice on
78 the Baffin shelf are not known.

79 On the basis of modeling, it has been proposed that Baffin Bay was blocked at its
80 southern end by an ice shelf extension of the Hudson Strait ice stream that grounded
81 across Davis Strait to reach southern Greenland, thus sealing Baffin Bay from the
82 Labrador Sea (Hulbe et al., 1997; Álvarez-Solas et al., 2010; Marcott et al., 2011). This
83 ice shelf was the starting point for modeling the processes that produce Heinrich events
84 (Hulbe et al., 1997; Álvarez-Solas et al., 2010; Marcott et al., 2011), but physical
85 evidence for it has not been recovered. An ice shelf of this scale would have
86 environmental consequences that should be recorded in Baffin Bay sediments. Firstly,
87 grounding of a Labrador Sea ice shelf along Davis Strait would prevent seawater
88 exchange between Baffin Bay and the Labrador Sea, excluding advection of organic
89 matter into Baffin Bay. It also would shut down *in situ* primary marine productivity in
90 Baffin Bay so that planktic and benthic organisms, their biomarkers, and bioturbation
91 would be absent in the sediment. Secondly, ice shelves and even extensive sea-ice cover
92 are known to restrict the movement and export of icebergs (Reeh et al., 2001; Domack
93 and Harris, 1998). Thus iceberg rafting and mixing of sediments of various provenances
94 in Baffin Bay would be reduced. Using these concepts, we test the LGM Baffin Bay ice-
95 shelf hypothesis by studying the sedimentological and biological characteristics of
96 sediments in HU2008029-12PC from the continental slope off western Greenland, a core
97 that extends from the LGM into the Younger Dryas (YD) and that recorded retreat of the
98 Greenland Ice Sheet during deglaciation (Jennings et al., 2017).

99

100 **2. Setting of core HU2008029-12PC**

101 Detailed studies of LGM and deglacial environments in Baffin Bay have been hampered
102 by relatively slow sediment accumulation rates and poor calcium carbonate preservation
103 (cf. Aksu, 1985; de Vernal et al., 1992; Simon et al., 2012). HU2008029-12PC (hereafter
104 called 12PC) was raised from the northern side of the Disko trough mouth fan (TMF)
105 from acoustically stratified sediments with continuous parallel reflections on the eastern
106 side of Baffin Bay (68°13.69' N; 57°37.08' W; 1475 m water depth; Campbell and de
107 Vernal, 2009) (Figs. 1 and 2). This site on the trough mouth fan has higher sediment
108 accumulation than sites in the deep basin of Baffin Bay that have variable sedimentation
109 rates that range between 3 and 35 cm/ka (Andrews et al., 1998; Hillaire-Marcel et al.,
110 1989, 2004; Simon et al., 2012; 2014) (Fig. 1).

111 The Disko TMF was built throughout the Quaternary by rapid sediment
112 deposition in front of the fast flowing Disko ice stream (Fig. 1) when the GIS margin was
113 extended on the shelf, and from hemipelagic sedimentation during and after ice retreat
114 (ÓCofaigh et al., 2013a, b; Jennings et al., 2017; Hofmann et al., 2016). An ice sheet
115 grounded at or near the shelf edge delivers abundant sediments directly to the continental
116 slope in the form of sediment gravity flows, including turbidity currents that form graded
117 sand layers, stratified sand/silt beds, and glaciogenic debris flows (ÓCofaigh et al., 2013a,
118 b, Lucci and Rebesco, 2007). Turbid meltwater plumes released from the ice front
119 produce plumites, which are finer grained than the turbidites as the sand is dropped near
120 the ice front and the silt and clay continue offshore in suspension (Hesse et al., 1997;
121 Lucchi and Rebesco, 2007). Depending on sea surface conditions such as perennial sea
122 ice and/or ice shelves, icebergs would also deliver sediment to the slope as they melted

123 during their transit in Baffin Bay (Andrews et al., 1998; 2014; Jennings et al., 2014;
124 Simon et al., 2012; 2014; 2016; Sheldon et al., 2016).

125 The modern sea ice edge extends southeast to northwest within Baffin Bay and
126 sea ice cover is greater in the western than in the eastern half due to the influence of the
127 relatively warm and saline West Greenland Current that enters Baffin Bay from the
128 southeast (Tang et al., 2004; Münchow et al., 2015) (Fig. 1). The boundary between
129 lower salinity, sea-ice bearing, Arctic Surface Water (ASW) that passes from the Arctic
130 Ocean through the channels of the Canadian Arctic Archipelago into Baffin Bay and
131 Atlantic Waters of the West Greenland Current (WGC) moving northward along West
132 Greenland is oriented NE-SW and migrates through the year. The relatively warm, saline
133 Atlantic Water submerges beneath the ASW (Buch, 2000a, b) and forms the West
134 Greenland Intermediate Water (WGIW) (Fig. 1 inset) (Tang et al., 2004). During the
135 LGM, however, the circulation regime in Baffin Bay would have been different because
136 the southward flow of ASW into Baffin Bay was blocked by confluent ice sheets
137 grounded in the channels of the Canadian Arctic Archipelago until the early Holocene
138 (England, 1999; Zreda et al., 1999; Jennings et al., 2011a; Piénkowski et al., 2011).
139 Today, warm Atlantic Water carried in the WGC accesses the GIS margins via cross
140 shelf troughs and fjords, where the ice sheet terminates in the sea (Holland et al., 2008)
141 and promotes basal melting (Straneo et al., 2012). WGC Atlantic Water flow was
142 initiated as early as 14.4 cal ka BP off central West Greenland and is implicated in
143 Greenland Ice Sheet retreat from the LGM position at the shelf edge (cf. Knutz et al.,
144 2011; Sheldon et al., 2016; Jennings et al., 2017).

145

146 **3. Methods:**

147 3.1 Age Model

148 The age model for 12PC is based on 7 radiocarbon dates between 201 and 860 cm on the
149 arctic planktic foraminifer, *Neogloboquadrina pachyderma* (*sensu* Darling et al., 2006).

150 The dates were previously published in Jennings et al., (2017) (Table 1). Radiocarbon
151 dates were calibrated using the Marine13 curve (Reimer et al., 2013). OxCal version
152 4.2.4 (Ramsey and Lee, 2013) was used to compute an age/depth model (Fig. 3). An age
153 reversal in the upper 110 cm of the core limited the chronology to the interval from 200
154 cm to the base of the core (1130 cm). The age of the core base is assumed to be no older
155 than 26.5 ka BP, the beginning of the LGM (Clark et al., 2009). This assumed basal age
156 results in a large uncertainty in the modeled age of the base of the core (24 to 28 cal ka
157 BP). Given this basal age, we might expect to record Baffin Bay Detrital Carbonate
158 (BBDC) event BBDC3 that is found in central Baffin Bay from c. 23.5 to 25 cal ka BP
159 (Simon et al., 2016). A single data point with 20% NBB source at 21.5 cal ka BP may
160 represent BBDC2 (21 cal ka BP; Simon et al., 2016) although it is not associated with a
161 coarse clast-rich interval as would be expected if it represented a BBDC event (Andrews
162 et al., 1998; Simon et al., 2012; Jackson et al., 2017) (Fig. 3). The lack of an interval of
163 high NBB and IRD below 467 cm (16.2 cal ka BP) in 12PC indicates that BBDC2 and
164 BBDC3 were not recovered in 12PC. Either these two events were not deposited basin
165 wide or the basal age of 12PC is younger than the 21 ka BP age of BBDC2. Given that
166 the deepest radiocarbon age in 12PC is 21.8 cal ka BP ($\Delta R=140$ years) and there are 3
167 meters of sediment below this depth in the core, we suggest it is more likely that BBDC2
168 and 3 were not deposited basin wide. Without additional information we continue with

169 the assumption that the core base is no older than the beginning of the global LGM of
170 26.5 ka BP (Clark et al., 2009).

171 We initially built the age model assuming a marine reservoir offset (ΔR) of
172 140 ± 30 years based on recent work in Disko Bugt (Lloyd et al., 2011), for consistency
173 with other central West Greenland sediment core records (cf Jennings et al., 2014; 2017;
174 Jackson et al., 2017; Hogan et al., 2016; Sheldon et al., 2016), and we note that prior to
175 2011, many publications used a $\Delta R=0$ years (Andrews et al., 1998; Knudsen et al., 2008).
176 However, recognizing that the marine reservoir offset could be large and variable over
177 the time interval of 12PC and because this core extends into the LGM, defined here as
178 beginning at 26.5 ka (Clark et al., 2009) and ending at the beginning of the Oldest Dryas
179 period, 18 ka BP (Buizert et al., 2014), we used the variable North Atlantic R values in
180 Stern and Lisiecki (2013) to provide an envelope of calibrated age so that we could
181 consider the correlations of boundaries and conditions recorded in the core with
182 established climatic intervals (Fig. 3f). To accomplish this we first calibrated each date
183 with $\Delta R=0$ ^{14}C years, which provides the maximum age. We then used the $\Delta R=0$ ages to
184 identify the appropriate 500 year bin of maximum, average and minimum R values from
185 Table S1 of Stern and Lisiecki (2013) and calibrated each of the dates using these three
186 R-values. The resulting envelope of ages, from $\Delta R=0$ to the maximum Stern and Lisiecki
187 2013 R-value, illustrates how the choice of ΔR affects correlation of boundaries in the
188 core with climate intervals from LGM through the YD (Fig. 3f; Table 1). Regardless,
189 these results confirm that the core contains LGM and Heinrich Stadial 1 (aka Oldest
190 Dryas) sediments, a key requirement for testing the ice shelf model (Hulbe et al., 1997;
191 Álvarez-Solas et al., 2010; Marcott et al., 2011).

192

193 3.2 Foraminiferal analyses.

194 One-cm wide samples were weighed wet and sieved on a 63- μm screen. Material >63
195 μm was kept wet in a storage solution of 70% distilled water and 30% ethanol with
196 baking soda as a buffer. Foraminifera were counted wet to prevent destruction of fragile
197 tests that disintegrate under the stress of drying. A wet splitter was used when necessary
198 to achieve a count of 200-300 benthic foraminifers and as many planktic foraminifers
199 as were in the benthic split. In most cases the full sample was counted. Equivalent dry
200 weights of the foram samples were estimated from sedimentology samples from the same
201 depths that had both wet and dry weights, allowing foraminifera/gram sediment to be
202 calculated.

203

204 3.3 Stable isotope analyses

205 Stable oxygen and carbon isotopes were measured on the planktic foram species
206 *Neogloboquadrina pachyderma* picked from the 150-250 μm size fraction in 41 samples;
207 results from 3 samples were rejected because they yielded a low signal. Samples $>100 \mu\text{g}$
208 have standard deviations of 0.01 and 0.03 ‰ for $\delta^{13}\text{C}$ and $\delta^{18}\text{O}$ respectively. Samples
209 weighing $<100 \mu\text{g}$ are reported with a standard deviation of 0.06 ‰ for $\delta^{13}\text{C}$, and an error
210 of ± 0.2 ‰ for $\delta^{18}\text{O}$. The oxygen isotope values are expressed as ‰ vs VPDB. Between
211 1050 and 857 cm all samples were of small weight but otherwise seemed reliable.
212 Measurements were made on a Micromass IsoprimeTM dual inlet coupled to a
213 MulticarbTM system at the Light Stable Isotope Geochemistry Laboratory at the
214 University of Montréal – UQAM.

215

216 3.4 CT scan.

217 CT scanning of the half round core was performed at the sediment core laboratory at the
218 University of Quebec at Rimouski. A CT number (a measure of sediment density) was
219 extracted from the images. The CT scan image was used to determine lithofacies and
220 boundaries, sedimentary structures, and to identify bioturbation, a key source of evidence
221 for the presence of benthic organisms and a source of information about sedimentation
222 rate variations between the radiocarbon dates (Wetzel, 1991). Counts of >2 mm clasts
223 interpreted as ice rafted detritus (IRD) were made from the CT images by counting in a 2
224 cm wide window across the core width continuously along the core length (Grobe, 1987).

225

226 3.5 Biomarkers: IP₂₅ and Brassicasterol

227 Biomarker analyses (IP₂₅ and brassicasterol) were performed using methods described
228 previously (Belt et al., 2012; Belt et al., 2015). Briefly, 9-octylheptadec-8-ene (9-OHD,
229 10 µL; 10 µg mL⁻¹) and 5α-androstan-3β-ol (10 µL; 10 µg mL⁻¹) were added to ca. 1 – 2
230 g of each freeze-dried sediment sample prior to extraction to permit quantification of IP₂₅
231 and sterols, respectively. Samples were then extracted using dichloromethane/methanol
232 (3 x 3 mL; 2:1 v/v) and ultrasonication. Following removal of the solvent from the
233 combined extracts using nitrogen, the resulting total organic extracts (TOE) were purified
234 using column chromatography (silica) with IP₂₅ (hexane; 6 mL) and brassicasterol (20:80
235 methylacetate/hexane; 6 mL) collected as two single fractions. Non-polar lipid fractions
236 were further separated into saturated and unsaturated hydrocarbons using glass pipettes
237 containing silver ion solid phase extraction material (Supelco Discovery® Ag-Ion).
238 Saturated hydrocarbons were eluted with hexane (1 mL), while unsaturated hydrocarbons

239 (including IP₂₅) were eluted with acetone (2 mL). All fractions were dried under a stream
240 of nitrogen.

241 Analysis of individual fractions was carried out using gas chromatography - mass
242 spectrometry (GC-MS) with operating conditions as described previously (e.g. Belt et al.,
243 2012; Brown and Belt, 2012). Sterols were derivatized (BSTFA; 50 µL; 70 °C; 1 h) prior
244 to analysis by GC-MS. Mass spectrometric analysis was carried out in total ion current
245 (TIC) and single-ion monitoring (SIM) modes. Individual lipids were identified on the
246 basis of their characteristic GC retention indices and mass spectra obtained from
247 standards. Quantification of IP₂₅ was achieved by dividing its integrated GC-MS peak
248 area by that of the internal standard (9-OHD) in SIM mode (both *m/z* 350) and
249 normalizing this ratio using an instrumental response factor (obtained from laboratory
250 standards of each analyte) and the mass of sediment (Belt et al., 2012). Analytical
251 reproducibility (6 %, n = 3) was monitored using a sediment with a known concentration
252 of IP₂₅. Brassicasterol concentrations were obtained by comparison of their respective
253 peak areas in SIM mode (brassicasterol, *m/z* 470) with those of the internal standard (*m/z*
254 333) and normalized as per IP₂₅.

255

256 3.6 Quantitative X-ray diffraction Mineralogy

257 Quantitative x-ray diffraction (qXRD) analyses were used to identify shifts in sediment
258 sources between ‘local’ West Greenland (WG) and ‘distal’ Northern Baffin Bay (NBB).
259 Samples for qXRD analysis were taken at 10 to 20 cm intervals throughout the core.
260 Sediment samples were freeze-dried and processed at INSTAAR using the method
261 described by Eberl (2003) and Andrews and Eberl (2011). The qXRD samples were

262 analysed on a Siemens D5000 XRD unit at a 0.02 2- θ step with a 2 second count;
263 minerals were identified using the program RockJock v.6 (Eberl, 2003). The qXRD 2-
264 source data to 17.5 cal ka BP is presented in Jennings et al. (2017). The determination of
265 sediment provenance is based on the quantitative X-ray diffraction (qXRD) analysis of
266 the < 2 mm surface and core sediments using the method outlined by Eberl (2003) and
267 described in more detail for our area by (Andrews and Eberl, 2012; Andrews et al., 2014;
268 O'Cofaigh et al., 2013a; Simon et al., 2014). We use the Excel macro unmixing program
269 "SedUnMix" (Eberl, 2004; Andrews and Eberl, 2012) to ascribe sediment mineral
270 assemblages to probable source areas. In this present study we discriminated between
271 two glacial derived sources; first a regional West Greenland source dominated by specific
272 ranges in quartz, plagioclase, k-feldspars and other non-clay and clay minerals, versus a
273 North Baffin Bay detrital carbonate source dominated by dolomite (Andrews et al., 2014;
274 O'Cofaigh et al., 2013; Jennings et al., 2017).

275

276 **4. Results and Interpretation**

277 4.1 Lithofacies Characteristics

278 There are two main lithofacies units defined by the sediment parameters in 12PC
279 (Fig. 3). The boundary between the two units (Fig. 4b) is well expressed by an abrupt
280 shift to lower CT# (Fig. 3A). This transition dates to 16.2 cal ka BP using $\Delta R=140$ years
281 and has been interpreted to represent the retreat of the Greenland Ice Sheet from the shelf
282 edge (Jennings et al., 2017). However, the full age-envelope ranges between 16.4
283 ($\Delta R=0$) to 14.0 (Max R) ka, or, late in Heinrich Stadial 1 to the end of the Bølling (Fig.
284 3f). Calibrated radiocarbon dates (Fig. 3F; $\Delta R=140$, pink) in the lower unit range from

285 21.8 to 16.2 cal ka BP. The lower three radiocarbon dates fall within the LGM regardless
286 of the marine reservoir age selected (Fig. 3F). The radiocarbon date at 571.5 cm falls
287 within Heinrich Stadial 1 regardless of the marine reservoir age (Fig. 3F).

288 The lower lithofacies unit, which represents the period when the ice sheet
289 grounding line was at or near the shelf edge, has higher magnetic susceptibility (Fig. 3C),
290 variable sand content including high weight percentage peaks (Fig. 3D) and a west
291 Greenlandic sediment composition (Fig. 3E) but rare >2mm clasts (Fig. 3B). From the
292 base of the core to 1022 cm, sediments are laminated mud with straight, sharp contacts
293 defining the laminae and vertically oriented burrows (Fig. 4f). Between 1025 and 768 cm
294 the sand content increases and stratification is disrupted by bioturbation (Fig. 3E).
295 Stratified mud with distinct vertical burrows extends from 768 to 735 cm (Fig. 3D). From
296 735 cm to 688 cm sand content increases. This sandy unit is overlain by another
297 sequence of stratified mud with distinct burrows between 688 and 630 cm. The sediment
298 between 630 and 467 cm is bioturbated, stratified mud with layering disturbed by
299 bioturbation (Fig. 4c). The uppermost part of this unit has high sand content and marks
300 the transition to the upper lithofacies unit.

301 The upper lithofacies from 467 to 0 cm, which represents deglaciation and the
302 Holocene (Jennings et al., 2017), has overall lower CT number (lower density) (Fig. 3A),
303 lower magnetic susceptibility (Fig. 3C) and generally lower sand content (Fig. 3D). But,
304 it has much higher numbers of >2mm clasts (IRD) (Fig. 3B). Immediately above the
305 boundary the sediments are low-density bioturbated mud with the sand fraction
306 comprising *Coscinodiscus* planktic diatoms and setae of *Chaetoceras*, consistent with the
307 low MS values (Fig. 3c). Well-defined, thin laminae and rare IRD occur at the base of the

308 unit, but transition upward to less-well defined laminae and rare to absent IRD from 420
309 cm to 352 cm. This fine interval was interpreted to record a period in the initial
310 deglaciation as the grounding line retreated off the shelf edge with retention of an ice
311 shelf (Jennings et al., 2017). At 352 cm (marked by middle horizontal blue line on Figure
312 3) the CT # (density), MS and sand increase (Fig. 3A, B, C, D). This level marks the start
313 of renewed retreat of the GIS grounding line by calving (Jennings et al., 2017). The
314 sediments are bioturbated but stratification is still evident, suggesting moderate
315 sedimentation rates. Apart from a peak in >2mm clasts of west Greenland provenance at
316 330 cm the main rise in >2mm clasts coincides with the entry of the Northern Baffin Bay
317 sediment source (NBB source) at 290 cm (Fig. 3B, E). Bioturbated, pebbly mud
318 associated with a rise in NBB provenance occurs between 280 and 175 cm with the
319 highest IRD interval from 280-240 cm (Fig. 3B, E). This NBB DC interval has been
320 found in several cores on the central West Greenland slope (Sheldon et al., 2016;
321 Jennings et al., 2017; Jackson et al., 2017) and has been correlated to BBDC1 (Simon et
322 al., 2012; 2014; Jackson et al., 2017), marking the retreat of NBB ice streams. The NBB
323 DC event is overlain by bioturbated mud with small, dispersed IRD and discontinuous silt
324 stringers between 175 and 152 cm. Bioturbated pebbly mud between 152 and 52 cm has
325 high NBB provenance between 160 and 90 cm, an interval that contains an age reversal
326 and a mixture of radiocarbon ages (Fig. 3F). The age reversal suggests that the upper
327 NBB peak is reworked. The upper 52 cm of the core is bioturbated mud with dispersed
328 IRD likely represents the middle to late Holocene time period, although it is undated.

329

330 4.2 Biological Proxies

331 Biological proxy data are expressed against age using the age model based on $\Delta R=140$
332 yrs (Fig. 5).

333 *4.2.1 Bioturbation*

334 The CT scan image (Fig. 3) reveals that the entire core is bioturbated, indicating
335 that there was sufficient oxygenation and food to support the benthos in Baffin Bay
336 throughout the time period represented by the core (Löwemark et al., 2012). Variations
337 in burrow shape and density are indicative of the interplay between oxygenation,
338 sedimentation rate, sedimentation processes, substrate consistency and food supply
339 (Reineck and Singh, 1980, Wetzel, 1991; Löwenmark et al., 2012) (Fig. 4). Intensely
340 bioturbated intervals in which sand layers are disrupted by burrowing (e.g. Fig. 4a, c, e)
341 suggest periods of relatively slow sedimentation (Wetzel, 1991), whereas intervals of
342 vertical burrows terminated by overlying strata (e.g. Fig. 4d, f) indicate episodic rapid
343 sedimentation (Jennings et al., 2011a). Figure 4 shows expanded views of segments of
344 the CT image shown in full on Figure 3 to illustrate some of the key lithofacies
345 characteristics and trace fossil types that provide evidence for sedimentation processes.
346 Muddy intervals typically have vertical burrows that are truncated by subsequent strata
347 (Fig. 4d). These mud intervals likely represent plumites deposited from turbid meltwater
348 plumes, whereas the sandy, stratified intervals with varying degrees of bioturbation likely
349 represent distal turbidites (Ó Cofaigh and Dowdeswell, 2001) (Fig. 4c, f).

350 *4.2.2 Foraminifera and Stable Isotopes*

351 The Foraminiferal abundances in 12PC are spiky, with intervals of low benthic and
352 planktic numbers per gram of dry sediment punctuated by periods of much higher
353 numbers of foraminifers per gram (Fig. 5D). The high variability in abundance relates to

354 variations in marine productivity, overprinted by carbonate dissolution, and dilution by
355 high (12.8 cm/ka on average from 250-860 cm) and varying sedimentation rates. The
356 lithofacies characteristics suggest widely varying sedimentation rates in the core that are
357 not captured by the less frequent age control. Therefore we did not attempt to calculate
358 foraminiferal flux, which would have been a more direct measure of productivity, but
359 rather rely on foraminiferal numbers per gram as a measure of productivity.

360 *N. pachyderma*, the only planktic species, forms abundance spikes up to 1620
361 specimens/g, with intervening periods of very low abundance to absence (Fig. 5). The
362 planktic forams were quite small from the base of the core to 860 cm (22 cal ka BP), but
363 increased in size above that level. In general the planktic and benthic foram abundances
364 rise and fall together, suggesting that the abundance spikes represent *in situ* productivity
365 and a link between surface productivity and benthic food supply, although we cannot
366 control for variations in carbonate preservation. Low numbers of *N. pachyderma* per
367 gram are consistent with low productivity under perennial sea ice and the high numbers
368 per gram are consistent with periods of more open water, such as leads or polynyas in
369 summer (e.g. Nørgaard-Pedersen et al., 2003). Advection of planktic foraminifers from
370 outside Baffin Bay is unlikely, especially given the linkage between the benthic and
371 planktic productivity (cf Knutz et al., 2011; Nørgaard-Pedersen et al., 2003).

372 Oxygen isotope values on *N. pachyderma* ranged between 5.4 and 2 ‰. The
373 interval between 22 and 18.2 cal ka BP has mostly heavy values that fall between 4 and 5
374 ‰ (Fig. 5), comparable to MIS 2 values in the Fram Strait (Nørgaard-Pedersen et al.,
375 2003). A shift to lighter $\delta^{18}\text{O}$ and $\delta^{13}\text{C}$ values begins at 18 cal ka BP, suggests reduced
376 ventilation (Sarnthein et al., 1995). This interval falls within HS1 regardless of which ΔR

377 is applied (Fig. 2; Table 1). Above this shift the $\delta^{18}\text{O}$ values remain above 3.7 ‰. A
378 pronounced light $\delta^{18}\text{O}$ spike at 19.4 cal ka BP corresponds to high planktic abundance
379 and increased IP₂₅ and Brassicasterol (Fig. 5). Oxygen isotopic values of this magnitude
380 can either be related to glacial meltwater, especially if they are paired with light $\delta^{13}\text{C}$
381 values (Sarnthein et al., 1995) or to increased rate of sea-ice production that can produce
382 brines with a light isotopic signature (Hillaire-Marcel et al., 2004; Hillaire-Marcel and de
383 Vernal, 2008). The overall trend in the $\delta^{13}\text{C}$ values is toward heavier values suggesting
384 better ventilation at the top of the record than at the bottom (Fig. 5).

385 The benthic foraminiferal assemblages (Fig. 6) provide insights into the
386 productivity of surface waters, stratification of the water column, and turbid glacial
387 meltwater influx. For example, sea-ice edge migration, either seasonal or in the form of
388 leads or polynyas, produces pulses of phytoplankton production that sink to the seabed,
389 providing food for benthic communities. The three most common benthic foraminiferal
390 species in 12PC are *Stainforthia feylingi*, *Cassidulina reniforme* and *Elphidium*
391 *excavatum* forma *clavata*. *S. feylingi* is dominant in conditions of stratified water column
392 with a cold freshwater lid and has been associated with productivity at the seasonal sea
393 ice edge (Seidenkrantz, 2013). It has been found in high abundances associated with
394 biosiliceous sediments (Jennings et al., 2006). *E. excavatum* and *C. reniforme* occur
395 together in glacial marine settings (Hald and Korsun, 1997). *C. reniforme* is also
396 considered to represent chilled Atlantic Water (Slubowska et al., 2005) and is found in
397 areas of relatively high, stable salinities (Polyak et al., 2002). *E. excavatum* is an
398 opportunistic species that thrives in unstable environmental conditions influenced by
399 rapid sedimentation and fluctuating salinities from turbid meltwater plumes (Hald and

400 Korsun, 1997). The agglutinated species, *Spiroplectammina biformis*, which occurs
401 mainly in the lower lithofacies unit is found in arctic fjords with strong meltwater signal
402 (Jennings and Helgadottir, 1994; Schaffer and Cole, 1986).

403 Several species indicative of marine productivity associated with nutrient rich
404 Atlantic Water occur in both the lower and upper lithofacies unit: *Melonis barleeanus*,
405 *Buccella frigida*, *Nonionella turgida* and *Nonionellina labradorica*. *Islandiella norcrossi*
406 and *I. helenae* both are arctic species, but *I. helenae* is associated with sea-ice edge
407 productivity while *I. norcrossi* reflects chilled Atlantic Water of normal marine salinity
408 (Polyak et al., 2002; Wollenburg et al., 2004; Lloyd, 2006). *I. norcrossi* is a common
409 calcareous species on the west Greenland shelf associated with Atlantic Water in the
410 West Greenland Current (e.g. Lloyd, 2006; Perner et al., 2012).

411 Near the top of the lower unit (16.5 cal ka BP), and continuing into the base of the
412 overlying biosiliceous mud, several species associated with marine productivity and
413 nutrient rich Atlantic Water spike to high percentages. These include *N. turgida*, *M.*
414 *barleeanus*, *B. frigida*, *I. norcrossi* and very low percentage of *Pullenia bulloides*.
415 Current indicator species, *Cibicides lobatulus* also increases at this boundary. The central
416 part of the diatom-rich mud is barren of calcareous foraminifers and is characterized by
417 low faunal abundances dominated by agglutinated foraminiferal species (e.g. *Textularia*
418 *earlandi*), suggesting that dissolution of carbonate likely overprinted the assemblages.
419 The upper part of the diatom-rich mud shows a return of several of the marine
420 productivity species along with increased percentages of *P. bulloides*, a chilled Atlantic
421 water species, that is common on the SE Greenland and Northern Iceland shelves under

422 conditions of strong Irminger Current Atlantic water inflow (Eiríksson et al., 2000;
423 Jennings et al., 2011b).

424 Above the diatom-rich mud, the percentages of *N. labradorica* and *I. norcrossi*
425 increase, and *S. feylingi* continues with high percentages. The chilled Atlantic Water
426 species, *Cassidulina neoteretis*, is abundant at the top of the dated section along with *I.*
427 *norcrossi*, consistent with intermediate Atlantic Water and less prominent glacial
428 meltwater influence (Jennings and Helgadottir, 1993). The gap in foraminifers between
429 12 and 13.9 cal ka BP is likely a consequence of carbonate dissolution as other cores
430 from the central West Greenland margin, but in slightly shallower water (JR175-VC29;
431 Fig. 1) have *C. neoteretis* continuously between 14 and 11 cal ka BP (Jennings et al.,
432 2017).

433 4.2.3 Biomarkers

434 Further evidence of marine productivity and sea ice comes from the algal biomarkers
435 brassicasterol and IP₂₅ (Fig. 5). In general, the presence of IP₂₅ indicates release from
436 melting seasonal sea ice (Fahl and Stein, 2012; Belt et al., 2013), while the absence of
437 IP₂₅ is consistent with intervals of thick perennial sea ice cover or no ice cover at all (Fahl
438 and Stein, 2012). Brassicasterol implies productivity in open-water conditions, but it also
439 can come from melting sea ice (Belt et al., 2013). In addition, the occurrence of polynyas
440 has been given as a possible reason for presence of IP₂₅ and brassicasterol under
441 otherwise heavy ice conditions, even in the central Arctic Ocean (Xiao et al., 2013).

442 In the lower, high CT lithofacies unit of 12PC, brassicasterol and IP₂₅ are present
443 in low abundances from 26 to 22 ka ($\Delta R=140$ yrs), coinciding with low foraminiferal
444 abundances (Fig. 5). Between 22 and 20 ka, brassicasterol rises but IP₂₅ is low to absent.

445 Foraminiferal abundances rise in this interval and the benthic fauna is characterized by
446 productivity species (*B. frigida*, *I. helenae*, *M. barleeanus* and *N. labradorica*). An
447 overall rise in IP₂₅ and a large peak in brassicasterol occur at 19.5 ka, and continue with
448 moderate values until another rise in brassicasterol values within the diatom-rich mud
449 unit (16.2 to 15.1 cal ka BP). Both IP₂₅ and brassicasterol continue to rise after 15.1 cal
450 ka BP, but IP₂₅ in particular rises to values unprecedented in the core after 14.3 cal ka BP.

451 This pattern of presence of IP₂₅ and brassicasterol in the lower lithofacies unit
452 argues for seasonal sea ice and some open water, although the generally low
453 concentrations suggest that these were both likely less than in the upper unit - probably
454 due to more extensive ice cover and only periodic opening - possibly as leads or
455 polynyas. As the final increase in IP₂₅ beginning at 16.2 ka is accompanied by rising,
456 high brassicasterol it likely points to development of a marginal ice zone where there is
457 increased marine productivity with probably more seasonal sea ice presence than before.

458

459 **5. Discussion**

460 5.1 Did an LGM Ice Shelf cover Baffin Bay?

461 There has been limited research on the LGM within Baffin Bay, which explains
462 how the Baffin Bay ice shelf concept has remained untested. Radiocarbon dates on
463 planktic foraminifers indicate that other cores besides 12PC have planktic fauna in the
464 LGM. Andrews et al (1998) obtained a pair of AMS ¹⁴C dates from abundant planktic
465 foraminifera in southern Baffin Bay core HU77029-017PC (17,990 ± 110, and 17,930 ±
466 210 ¹⁴C yrs; Andrews et al., 1998) (Fig. 1). These ¹⁴C ages calibrate to the LGM (~21 ka
467 BP; ΔR=140 years). A ¹⁴C date on planktic foraminifers from core HE006-4-2PC

468 (21,440± 140 ¹⁴C yrs) on the northern side of the Uummannaq TMF (Fig. 1) calibrates to
469 ~25 ka BP ($\Delta R=140$ years) (Ó Cofaigh et al., 2013a). In the LGM interval of 12PC (1130
470 cm to at least 690 cm) when the modeled Baffin Bay ice shelf would be in place, there
471 are multiple lines of evidence for biological activity, including bioturbation, algal
472 biomarkers and benthic and planktic foraminifers (Figs. 3 - 6). These findings are
473 consistent with perennial sea-ice cover with some open water in the form of leads or
474 polynyas on the eastern side of Baffin Bay. Full ice-shelf cover from an ice shelf
475 extending from the Hudson Strait ice stream and grounding on Davis Strait all the way to
476 Greenland (Alvarez-Solas et al., 2010; 2011; Marcott et al., 2011) would not allow the
477 surface productivity (e.g. algal biomarkers, planktic forams) in Baffin Bay that would be
478 needed to feed the benthic organisms that are evident (bioturbation and benthic
479 foraminifers). On this basis we reject the modeling result of a full Baffin Bay ice shelf.
480 While life has been observed under modern ice shelves in Antarctica, it is dependent on
481 strong ocean inflow to the sub ice-shelf cavity from outside the ice shelf (Post et al.,
482 2014). In the case of the Baffin Bay ice shelf cover as it is modeled, it would be sealed
483 from the Labrador Sea marine advection and food supply.

484 The idea of the Davis Strait grounded ice shelf sprang in part from efforts to test a
485 mechanism for Heinrich Event 1 (H1), in which subsurface warming reconstructed in the
486 N. Atlantic in response to reduced Atlantic meridional overturning circulation (AMOC)
487 during HS1 (McManus et al., 2004) weakens a buttressing ice shelf fronting the Hudson
488 Strait ice stream and produces a Heinrich event (Álvarez-Solas et al., 2010; 2011;
489 Marcott et al., 2011). Hulbe et al. (2004) modified their original 1997 Labrador Sea ice
490 shelf idea to support instead fringing ice shelves along the coasts in Eastern Canada that

491 were proposed to have met their demise through a process of meltwater infilling of
492 surface crevasses. The existence of this type of ice shelf and H-event process has been
493 contested (Alley et al., 2005), but it is more consistent with the 12PC data than the
494 original idea of an ice shelf grounding on Davis Strait (Hulbe et al., 1997).

495 *5.2 Heinrich Stadial Environments*

496 The data in 12PC allow examination of the environmental response in Baffin Bay
497 to the transition from LGM to HS1, and the response in Baffin Bay to the large ice
498 discharge from Hudson Strait during H1 which occurred when subsurface ocean heat was
499 at a maximum and AMOC at a minimum (Marcott et al., 2011). Locating the LGM/HS1
500 transition and H1 in 12PC is made difficult by the uncertainties in the magnitude of the
501 local marine reservoir age through time (Fig. 3F) (Stern and Lisiecki, 2013). The
502 accepted timing of H1 calving event is 16.8 ka BP (Hemming, 2004), although it may be
503 closer to 16 ka BP based on the timing of the peak of IRD in the North Atlantic IRD
504 stack during HS1 (Stern and Lisiecki, 2013). If we apply the ΔR envelope approach using
505 data from Stern and Lisiecki (2013) to the mean value of the best 2 constraining
506 radiocarbon ages from the base of DC1 (=H1) in cores HU75009-IV-055PC and
507 HU87033-009 LCF (Fig. 1; Andrews et al., 1994; Jennings et al., 1996), from the
508 Labrador Sea, we obtain a range of ages for the event that spans HS1 (Table 1). The ΔR
509 that matches best the H1 16.8 ka age determined by Hemming (2004) is the lower ΔR
510 from Stern and Lisiecki (2013) (Table 1). On this basis, we chose to use the Lower ΔR to
511 determine where HS1 lies in the 12PC record. Lower ΔR places the base of HS1 (18 ka
512 BP) at 610 cm and its end (14.7 ka BP) at 395cm, right at the end of the diatom-rich mud
513 unit and before the initiation of calving retreat (Fig. 3F and 7). Lower ΔR also puts the

514 calving retreat and the timing of the west Greenland DC event (=BBDC1; Jackson et al.,
515 2017) (Fig. 3) in the Bølling/Allerød interstadial (Fig. 7). The age model calculated with
516 an invariant $\Delta R=140$ years places the lithofacies transition which represents the
517 grounding line retreat from the west Greenland shelf edge at 16.2 cal ka BP, within HS1
518 (Jennings et al., 2017), but places the end of HS1 after the initiation of GIS calving
519 retreat.

520 Figure 7 illustrates how key proxy data map into the Heinrich Stadial interval
521 defined by evidence of sluggish AMOC (McManus et al., 2004) using the lower ΔR of
522 Stern and Lisiecki (2013). In the Labrador Sea HS1 is an interval of anomalously warm
523 bottom waters (Marcott et al., 2011) within which H1 occurred (Fig. 7). We would
524 expect this massive freshwater (meltwater and icebergs) outflow from collapse of the
525 Hudson Strait ice stream (Andrews and Tedesco, 1992; Hesse and Khodabakhsh, 2016)
526 to perturb environments in Baffin Bay or initiate a transition to different
527 paleoceanographic conditions.

528 The transition to lighter $\delta^{18}\text{O}$ values and a shift to very high percentages of *S.*
529 *feylingi* coincide with HS1 (Fig. 7). This signal is also seen in nearby core JR175-VC29
530 (Fig. 1), from 900 m water depth (Jennings et al., 2017) and is associated in both 12PC
531 and VC29 with deposition of diatom-rich mud with rare IRD; a fine-grained unit of
532 similar age is observed in core GeoTü SL-170 (Jackson et al., 2017) slightly north of
533 VC29. The diatom-rich mud interval has been interpreted by Jennings et al. (2017) to
534 indicate exclusion of coarse sediment delivery to the Disko TMF by retention of a
535 fringing ice shelf after initial grounding line retreat. Overall, brassicasterol abundances
536 are low in HS1. A period of high productivity of benthic forams indicative of nutrient

537 rich Atlantic water at the subsurface (Fig. 5) (indicated on Fig. 7 by red stars and low
538 percentages of the benthic foraminiferal species, *S. feylingi*) coincides with the initial
539 GIS retreat from the shelf edge as indicated in the CT# profile (Jennings et al., 2017).
540 Subsequent interstadial conditions are marked by rising marine productivity, renewed
541 subsurface Atlantic Water influence, and renewed retreat of the GIS, followed by
542 development of consistent seasonal sea ice and release/melting of detrital carbonate
543 bearing ice bergs from ice margins of northern Baffin Bay termed a west Greenland DC
544 event by (Jennings et al., 2017) that has been shown to be correlative to BBDC1 (Simon
545 et al. (2016) by Jackson et al. (2017).

546

547 **6. Conclusions**

548 1. Based on the data presented we reject the hypothesis that Baffin Bay was covered by a
549 full ice shelf during the LGM. We conclude instead that Baffin Bay was perennially sea-
550 ice covered with nutrient rich, relatively warm Atlantic water present at depth through the
551 LGM. Evidence of marine productivity suggests that there were openings in the sea-ice
552 cover as leads and polynyas to support marine productivity. Concurrently, sediment-
553 laden, glacial-meltwater and turbidity currents were released from the GIS, grounded at
554 the shelf edge, but IRD was rare suggesting the ice front was protected by a fringing ice
555 shelf and/or the perennial sea-ice cover.

556 2. Reduced ventilation and productivity, coincident with a cold surface lid of meltwater
557 was established in HS1. After Heinrich Event 1, but within the Heinrich stadial, an
558 interval of increased productivity and Atlantic Water is associated with the retreat of the
559 GIS grounding line from the shelf edge.

560 3. The implication for Heinrich Events and Ocean warming/Ice Shelf hypothesis is that
561 perennial sea-ice cover and/or fringing ice shelves may be sufficient to explain the heat
562 retention and back-pressure proposed to explain the dynamics that produce Heinrich
563 Events.

564

565 **7. Acknowledgements**

566 Funding for this research was provided by the US National Science Foundation grant
567 ARC1203492 and the UK Natural Environment Research Council grant NE/D001951/1.
568 We thank the captain, crew and scientists aboard the 2008 CSS Hudson cruise HU2008-
569 029 for acquisition of core 2009029-12PC. We gratefully acknowledge the microscope
570 and x-ray diffraction research by undergraduate research assistants, Brian Shreve,
571 Jennifer Kelly, Matthew Reed, and Matthew Glasset. We thank Quentin Simon and one
572 anonymous reviewer for helpful critique of the manuscript.

573

574 **8. Figure Captions**

575 Figure 1. Bathymetric map centered on Baffin Bay (BB) showing the location of core
576 HU2008029-12PC (12PC) and other cores mentioned in the text, the distribution of
577 Paleozoic carbonate bedrock, mapped ice margin positions in northern Baffin Bay (Li et
578 al., 2011) and central west Greenland (Ó Cofaigh et al., 2013a) and major ice streams.
579 UIS = Uummannaq ice stream; DIS = Disko ice stream; SSIS = Smith Sound ice stream;
580 LSIS = Lancaster Sound ice stream. Northward flowing West Greenland Current (WGC)
581 is shown as the thin red line and the southward flowing Baffin Current (BC) is shown as
582 a thin blue line. The position of the acoustic profile in Figure 2 is shown as a black line.

583 HU2008029-016PC=16; HE006-4-2PC=2; JR175-VC29=29; HU77029-017PC=17;
584 HU75009-IV-055PC=55 and HU87033-009 LCF=9. Inset plot shows the salinity and
585 temperature against water depth at from the same location as 2008029-12PC.
586 ASW=Arctic Surface Water; WGIW=West Greenland Intermediate Water; DBBW=Deep
587 Baffin Bay Water.

588

589 Figure 2. A. 3.5 kHz sub-bottom profile over the site of 2008029-12PC demonstrating
590 the acoustically-stratified character of the seabed in the area. B. A zoom in map of the 3.5
591 kHz sub-bottom profile and the core location shown in Figure 1. The bathymetry is from
592 GEBCO.

593

594 Figure 3. Lithological proxies and age control for 2008029-12PC. A is the CT image
595 against depth in the core. Black bars along depth axis show the locations of CT images
596 shown in Figure 4. 'V' denotes locations of vertical burrows. B. IRD counts (>2mm
597 clasts) from CT scan in 2 cm increments. C. CT number, a measure of density derived
598 from the CT image. D. Magnetic Susceptibility measure by multi sensor track (MST). E.
599 Weight percentage of >63 μm sand fraction from foraminiferal samples. F. Two-source
600 provenance of minerals: Northern Baffin Bay (NBB, brown) vs. the local source, central
601 west Greenland (green). F. Depth-Age model in pink ($\Delta R=140\pm 30$ yrs) showing 1σ and
602 2σ uncertainties of the model. Excluded from the model are benthic foraminiferal ages
603 (green distributions) and outliers at 1 meter. Age envelope for other potential ΔR
604 calibrations are shown by blue ($\Delta R=0$); Red, green, orange = lower, mean, and upper ΔR
605 values from Stern and Lisiecki (2013). Climate units are along the age scale.

606

607 Figure 4. Examples of lithofacies and bioturbation types from 2008029-12PC CT scans.

608 See Figure 3 for locations of these examples on the CT image of the core.

609

610 Figure 5. Biological proxies from 12PC compared with CT# plot to assist with

611 comparison to depth on depth in Figure 3. A. CT#; B. sea ice biomarker, IP₂₅; C. marine

612 productivity biomarker, brassicasterol; D. Benthic (blue) and planktic (red) forams per

613 gram of dry sediment; E. $\delta^{18}\text{O}$ of planktic foraminifer, *N. pachyderma*, blue; F. $\delta^{13}\text{C}$ of *N.*

614 *pachyderma*, green.

615 Figure 6. Benthic foraminiferal species in 12PC. Green represent marine productivity

616 species; Red=Atlantic Water species; Blue = Arctic species; Light Blue; Glacial marine

617 species; Orange=transformed (cooler and slightly lower salinity) Atlantic Water species.

618

619 Figure 7. Comparison between Pa/Th record of AMOC (McManus et al., 2004) and the

620 timing of Heinrich Event 1 (H1) to key paleoenvironmental proxies in 12PC. The HS1

621 interval (yellow box) is defined in the core with use of the Lower ΔR of Stern and

622 Lisiecki (2013) (Fig. 3f). Blue lines show where key events in the core map into the

623 climatic intervals with use of the Lower ΔR of Stern and Lisiecki (2013). A. CT # from

624 12PC; B. Brassicasterol, 12PC; C. IP₂₅, 12PC; D. *Stainforthia feylingi*, 12PC; E. Oxygen

625 isotope ratios, 12PC; F. Pa/Th ratios (McManus et al., 2004).

626 **References Cited**

627

628 Aksu, A. E., 1985. Climatic and oceanographic changes over the past 400,000 years:

629 Evidence from deep-sea cores on Baffin Bay and David Strait. *In* Andrews, J. T. (ed.),

630 *Quaternary Environments: Eastern Canadian Arctic, Baffin Bay and Western*

631 *Greenland*. Boston: Allen and Unwin, 181-209.

632
633 Alley, R. B., Andrews, J. T., Barber, D. C., and Clark, P. U., 2005: Comment on
634 "Catastrophic ice shelf breakup as the source of Heinrich event icebergs" by C.L.
635 Hulbe et al. *Palaeoceanography*, 20: doi:10.1029/2004PA001086.
636
637 Álvarez-Solas, J., Charbit, S., Ritz, C., Paillard, D., Ramstein, G., and Dumas, C.: Links
638 between ocean temperature and iceberg discharge during Heinrich events, *Nature*
639 *Geoscience*, 3, 122–126, 2010
640
641 Álvarez-Solas, J., Montoya, M., Ritz, C., Ramstein, G., Charbit, S., Dumas, C.,
642 Nisancioglu, K., Dokken, T., Ganopolski, A., 2011. Heinrich event 1: an example of
643 dynamical ice-sheet reaction to ocean changes. *Climate of the Past* 7, 1297-1306.
644 doi:10.5194/cp-7-1297-2011.
645
646 Andrews, J.T., Eberl, D.D., 2011. Surface (sea floor) and near-surface (box cores)
647 sediment mineralogy in Baffin Bay as a key to sediment provenance and ice sheet
648 variations. *Can. J. Earth Sci.* 48 (9), 1307 - 1328. <http://dx.doi.org/10.1139/-11-021>.
649
650 Andrews, J.T., Eberl, D.D., 2012. Determination of sediment provenance by unmixing
651 the mineralogy of source-area sediments: The "SedUnMix" program. *Marine Geology*
652 291, 24-33.
653
654 Andrews, J.T., Erlenkeuser, H., Tedesco, K., Aksu, A., Jull, A.J.T., 1994. Late Quaternary
655 (Stage 2 and 3) Meltwater and Heinrich events, NW Labrador Sea. *Quaternary*
656 *Research* 41, 26-34.
657
658 Andrews, J.T., Gibb, O.T., Jennings, A.E., Simon, Q., 2014. Variations in the provenance
659 of sediment from ice sheets surrounding Baffin Bay during MIS 2 and 3 and export
660 to the Labrador Shelf Sea: site HU2008029-0008 Davis Strait. *Journal of Quaternary*
661 *Science* 29, 3-13.
662
663 Andrews, J. T., Kirby, M. E., Aksu, A., Barber, D. C., and Meese, D., 1998. Late
664 Quaternary Detrital Carbonate (DC-) events in Baffin Bay (67° - 74° N): Do they
665 correlate with and contribute to Heinrich Events in the North Atlantic? *Quaternary*
666 *Science Reviews*, 17: 1125-1137.
667
668 Andrews, J. T. and Tedesco, K., 1992: Detrital carbonate-rich sediments,
669 northwestern Labrador Sea: Implications for ice-sheet dynamics and iceberg rafting
670 (Heinrich) events in the North Atlantic. *Geology*, 20: 1087-1090.
671
672 Belt, S.T., Brown, T.A., Navarro Rodriguez, A., Cabedo Sanz, P., Tonkin, A., Ingle, R.,
673 2012. A reproducible method for the extraction, identification and quantification of
674 the Arctic sea ice proxy IP25 from marine sediments. *Analytical Methods* 4, 705-713.
675
676 Belt, S.T., Brown, T.A., Ringrose, A.E., Cabedo-Sanz, P., Mundy, C.J., Gosselin, M.,
677 Poulin, M., 2013. Quantitative measurement of the sea ice diatom biomarker IP25

678 and sterols in Arctic sea ice and underlying sediments: Further considerations for
679 palaeo sea ice reconstruction. *Organic Geochemistry* 62, 33–45.
680
681 Belt, S.T., Cabedo-Sanz, P., Smik, L., Navarro-Rodriguez, A., Berben, S.M., Knies, J.,
682 Husum, K., 2015. Identification of paleo Arctic winter sea ice limits and the marginal
683 ice zone: Optimised biomarker-based reconstructions of late Quaternary Arctic sea
684 ice. *Earth and Planetary Science Letters* 431, 127-139.
685
686 Blake, W., Jr. 1977. Glacial sculpture along the east-central coast of Ellesmere Island,
687 Arctic Archipelago. Current Research, Part C, Geological Survey of Canada, Paper 77-
688 1C, 107-115.
689
690 Briner, J. P., Miller, G. H., Davis, P. T., Bierman, P. R., and Caffee, M., 2003. Last Glacial
691 Maximum ice sheet dynamics in Arctic Canada inferred from young erratics perched
692 on ancient tors. *Quaternary Science Reviews*, 22: 437-444.
693
694 Brown, T.A., Belt, S.T., 2012. Closely linked sea ice–pelagic coupling in the Amundsen
695 Gulf revealed by the sea ice diatom biomarker IP25. *Journal of plankton research* 34,
696 647-654.
697
698 Buch E. 2000a. A monograph on the physical oceanography of the Greenland waters.
699 Danish Meteorological Institute Scientific Report, 00-12.
700
701 Buch E. 2000b. Air-sea-ice conditions off southwest Greenland, 1981–1997. *Journal*
702 *of Northwest Atlantic Fisheries Science* 26, 1–14.
703
704 Buizert, C., Gkinis, V., Severinghaus, J.P., He, F., Lecavalier, B.S., Kindler, P.,
705 Leuenberger, M., Carlson, A.E., Vinther, B., Masson-Delmotte, V., White, J.W.C., Liu, Z.,
706 Otto-Bliesner, B., Brook, E.J., 2014. Greenland temperature response to climate
707 forcing during the last deglaciation. *Science* 345, 1177-1180. DOI:
708 10.1126/science.1254961
709
710 Campbell, D C, de Vernal, A., 2009. CCGS Hudson Expedition 2008029: marine
711 geology and paleoceanography of Baffin Bay and adjacent areas, Nain, NL to Halifax,
712 NS, August 28-September 23. Geological Survey of Canada, Open File 5989, 2009,
713 212 pages; 1 DVD, doi:10.4095/261330
714
715 Clark, P.U., Dyke, A.S., Shakun, D., Carlson, A.E., Clark, J., Wohlfarth, B., Mitrovica, J.X.,
716 Hostetler, S.W., McCabe, A.M., 2009. The Last Glacial Maximum. *Science* 325, 710-
717 714.
718
719 Dahl-Jensen, D. and al., e., 1998: Past Temperatures Directly from the Greenland Ice
720 Sheet. *Science*, 282: 268-271.
721

722 Darling, K. F., Kucera, M., Kroon, D., Wade, C.M., 2006. A resolution for the coiling
723 direction paradox in *Neogloboquadrina pachyderma*. *Paleoceanography* 21,
724 PA2011, doi:10.1029/2005PA001189.

725

726 de Vernal, A., Bilodeau, G., Hillair -Marcel, C., Kassou, N., 1992. Quantitative
727 assessment of carbonate dissolution in marine sediments from foraminifer linings
728 vs. shell ratios: example from Davis Strait, NW North Atlantic, *Geology*, 20: 527-530.
729

730 Domack, E.W., Harris, P.T., 1998. A new depositional model for ice shelves, based
731 upon sediment cores from the Ross Sea and the Mac. Roberson shelf, Antarctica.
732 *Annals of Glaciology* 27, 281-284.
733

734 Dowdeswell, J.A., Hogan, K.A., Ó Cofaigh, C., Fugelli, E.M.G., Evans, J., Noormets, R.,
735 2014. Late Quaternary ice flow in a West Greenland fjord and cross-shelf trough
736 system: submarine landforms from Rink Isbrae to Uummannaq shelf and slope.
737 *Quat. Sci. Rev.* 92, 292-309. <http://dx.doi.org/10.1016/j.quascirev.2013.09.007>.
738

739 Dyke, A. S., Andrews, J. T., Clark, P. U., England, J. H., Miller, G. H., Shaw, J., and
740 Veillette, J. J., 2002: The Laurentide and Innuitian ice sheets during the Last Glacial
741 Maximum. *Quaternary Science Reviews*, 21, 9-31.
742

743 Eberl, D.D., 2003. User guide to RockJock: A program for determining quantitative
744 mineralogy from X-ray diffraction data. United States Geological Survey, Open File
745 Report 03-78, 40 pp, Washington, DC.
746

747 Eiríksson, J., Knudsen, K.L., Hafliðason, H., Henriksen, P., 2000. Late-glacial and
748 Holocene palaeoceanography of the North Icelandic shelf. *Journal of Quaternary*
749 *Science* 15, 23-42.
750

751 England, J. 1999. Coalescent Greenland and Innuitian ice during the Last Glacial
752 Maximum: Revising the Quaternary of the Canadian High Arctic. *Quaternary Science*
753 *Reviews* 18, 421–426, [http://dx.doi.org/10.1016/S0277-3791\(98\)00070-5](http://dx.doi.org/10.1016/S0277-3791(98)00070-5).
754

755 England, J., Atkinson, N., Bednarski, J., Dyke, A.S., Hodgson, D.A., Ó Cofaigh, C. 2006.
756 The Innuitian Ice Sheet: configuration, dynamics and chronology. *Quaternary*
757 *Science Reviews* 25, 689-703.
758

759 Fahl, K., Stein, R., 2012. Modern seasonal variability and deglacial/Holocene change
760 of central Arctic Ocean sea ice cover: New insights from biomarker proxy records.
761 *Earth and Planetary Science Letters* 351–352, 123–133.
762

763 Grobe, H., 1987. A simple method for the determination of ice-rafted debris in
764 sediment cores. *Polarforschung* 57 (3), 123-126.
765

766 Hald, M., Korsun, S. 1997. Distribution of modern benthic foraminifera from fjords of
767 Svalbard, European Arctic. *Journal of Foraminiferal Research* 27, 101–122.

768
769 Hemming, S.R., 2004. Heinrich events: massive late Pleistocene detritus layers of the
770 North Atlantic and their global climate imprint. *Rev. Geophys.* 42, RG1005.
771
772 Hesse, R., Khodabakhsh, S. 2016. Anatomy of Labrador Sea Heinrich layers. *Marine*
773 *Geology* 380, 44-86. <http://dx.doi.org/10.1016/j.margeo.2016.05.019>
774
775 Hesse, R., Khodabakhsh, S., Klauke, I., Ryan, WBF., 1997. Asymmetrical turbid
776 surface-plume deposition near ice-outlets of the Pleistocene Laurentide ice sheet in
777 the Labrador Sea. *Geo-Marine Letters*, 17, 179-187.
778
779 Hillaire-Marcel, C., de Vernal, A., 2008. Stable isotope clue to episodic sea-ice
780 formation in the glacial North Atlantic. *Earth and Planetary Science Letters*, 268,
781 143-150.
782
783 Hillaire-Marcel, C., de Vernal, A., Aksu, A.E., Macko, S., 1989. High-resolution
784 isotopic and micropaleontological studies of upper Pleistocene sediments at ODP
785 Site 645, Baffin Bay, *Proceedings of the Ocean Drilling Program*, 105B: 599-616.
786
787 Hofmann, J.C., Knutz, P.C., Nielsen, T., Kuijpers, A., 2016. Seismic architecture and
788 evolution of the Disko Bay trough-mouth fan, central West Greenland margin,
789 *Quaternary Science Reviews*, <http://dx.doi.org/10.1016/j.quascirev.2016.05.019>
790
791 Holland, D.M., Thomas, R.H., de Young, B., Ribergaard, M.H., Lyberth, B., 2008.
792 Acceleration of Jakobshavn Isbræ triggered by warm subsurface oceanwaters.
793 *Nature Geoscience* 1 (10), 659e664. <http://dx.doi.org/10.1038/ngeo316>.
794
795 Hulbe, C.L., 1997. An ice shelf mechanism for Heinrich layer production,
796 *Paleoceanography* 12, 711 -717.
797
798 Hulbe, C. L., MacAyeal, D. R., Denton, G. H., Kleman, J., and Lowell, T. V., 2004:
799 Catastrophic ice shelf breakup as the source for Heinrich event icebergs.
800 *Palaeoceanography*, 19: 1 of 15, doi.10.1029/2003:PA000890, 002004.
801
802 Jackson, R., Carlson, A.E., Hillaire-Marcel, C., Wacker, L., Vogt, C., Kucera, M., 2017.
803 Asynchronous instability of the North American-Arctic and Greenland ice sheets
804 during the last deglaciation. *Quaternary Science Reviews* 164, 140-153.
805 <http://dx.doi.org/10.1016/j.quascirev.2017.03.020>.
806
807 Jennings, A.E., Andrews, J.T., Ó Cofaigh, C., St. Onge, G., Sheldon, C., Belt, S.T., Cabedo-
808 Sanz, P., Hillaire-Marcel, C. 2017. Ocean forcing of Ice Sheet Retreat in Central West
809 Greenland from LGM through Deglaciation. *Earth and Planetary Science Letters* 472,
810 1-13 .
811

812 Jennings, A.E., Andrews, J.T., Wilson, L., 2011b. Holocene Environmental Evolution of
813 the SE Greenland Shelf North and South of the Denmark Strait: Irminger and East
814 Greenland Current Interactions. *Quaternary Science Reviews* 30: 980-998.
815
816 Jennings, A.E., Hald, M., Smith, L.M., and Andrews, J.T., 2006. Freshwater forcing
817 from the Greenland Ice Sheet during the Younger Dryas: Evidence from
818 southeastern Greenland shelf cores: *Quaternary Science Reviews* 25, 282–298,
819 doi:10.1016/j.quascirev.2005.04.006.
820
821 Jennings, A.E., Helgadottir, G., 1994. Foraminiferal assemblages from the fjords and
822 shelf of eastern Greenland. *J. Foraminifer. Res.* 24 (2), 123e144.
823 <http://dx.doi.org/10.2113/gsjfr.24.2.123>.
824
825 Jennings, A.E., Sheldon, C., Cronin, T.M., Francus, F., Stoner, J., Andrews, J., 2011a. The
826 Holocene history of Nares Strait, transition from glacial bay to Arctic-Atlantic
827 throughflow. *Oceanography* 24, no. 3, 26-41.
828
829 Jennings, A. E., Tedesco, K. A., Andrews, J. T., and Kirby, M. E., 1996. Shelf erosion and
830 glacial ice proximity in the Labrador Sea during and after Heinrich events (H-3 or 4
831 to H-0) as shown by foraminifera. In Andrews, J. T., Austin, W. E. N., Bergsten, H., and
832 Jennings, A. E. (eds.), *Late Quaternary Palaeoceanography of the North Atlantic*
833 *Margins*: Geological Society Special Publications, 29-49.
834
835 Jennings, A.E., Walton, M.E., Cofaigh, C._O., Kilfeather, A., Andrews, J.T., Ortiz, J.D., et
836 al., 2014. Paleoenvironments during Younger Dryas-early Holocene retreat of the
837 Greenland ice sheet from outer Disko Trough, central west Greenland. *J. Quat. Sci.* 29
838 (1), 27e40. <http://dx.doi.org/10.1002/jqs.2652>.
839
840 Kaufman, D.S., Williams, K.M. (compilers), 1992. Radiocarbon Date List VII: Baffin
841 Island, N.W.T., Canada. INSTAAR Occasional Paper 48. Institute of Arctic and Alpine
842 Research, University of Colorado, Boulder.
843
844 Knutz, P. C., M.-A. Sicre, H. Ebbesen, S. Christiansen, and A. Kuijpers, 2011. Multiple-
845 stage deglacial retreat of the southern Greenland Ice Sheet linked with Irminger
846 Current warm water transport, *Paleoceanography* 26, PA3204,
847 doi:10.1029/2010PA002053.
848
849 Li, G., Piper, D. J. W., and Campbell, D. C., 2011: The Quaternary Lancaster Sound
850 trough-mouth fan, NW Baffin Bay. *Journal of Quaternary Science*, 26: 511-522.
851 Lloyd, J. M. 2006. Modern distribution of benthic foraminifera from Disko Bugt, West
852 Greenland. *Journal of Foraminiferal Research* 36, 315–331.
853
854 Lloyd, J.M., Moros, M., Perner, K., Telford, R.J., Kuijpers, A., Jansen, E., et al., 2011.A
855 100 yr record of ocean temperature control on the stability of JakobshavnIsbrae,
856 West Greenland. *Geology* 39 (9), 867-870. <http://dx.doi.org/10.1130/G32076.1>.
857

858 Löwemark, L., O'Regan, M., Hanebuth, T.J.J., Jakobsson, M., 2012. Late Quaternary
859 spatial and temporal variability in Arctic deep-sea bioturbation and its relation to
860 Mn cycles. *Palaeogeography, Palaeoclimatology, Palaeoecology* 365-366, 192-208.
861

862 Lucci, RG and Rebesco, M., 2007. Glacial contourites on the Antarctic Peninsula
863 margin: insight for palaeoenvironmental and palaeoclimatic conditions. Geological
864 Society, London, Special Publications, 276: 111-127.
865

866 Marcott et al., 2011. Ice-shelf collapse from subsurface warming as a trigger for
867 Heinrich Events. *PNAS* 108. No. 33 p. 13415-13419
868

869 McManus, J.F., Francois, R., Gherardi, J.-M., Keigwin, L.D., Brown-Leger, S., 2004.
870 Collapse and rapid resumption of the Atlantic meridional circulation linked to
871 deglacial climate change. *Nature* 428, 834-837.
872

873 Münchow A., Falkner, A. Melling, H., 2015. Baffin Island and West Greenland Current
874 Systems in northern Baffin Bay. *Progress in Oceanography* 132, 305–317
875

876 Ó Cofaigh C., Andrews JT, Jennings AE, Dowdeswell JA, Hogan KA, Kilfeather AA, et
877 al. (2013a) Glacimarine lithofacies, provenance and depositional processes on a West
878 Greenland trough-mouth fan. *Journal of Quaternary Science* 28. Available at:
879 <http://dx.doi.org/10.1002/jqs.2569>: doi:10.1002/jqs.2569.
880

881 Ó Cofaigh C, Dowdeswell J.A., 2001. Laminated sediments in glacimarine environments:
882 diagnostic criteria for their interpretation. *Quaternary Science Reviews* 20, 1411-1436.
883

884 Ó Cofaigh C., Dowdeswell J.A., Jennings A.E., Hogan K.A., Kilfeather A., Hiemstra
885 J.F., et al. (2013b) An extensive and dynamic ice sheet on the West Greenland shelf
886 during the last glacial cycle. *Geology* 41(2): 219–222: doi:10.1130/G33759.1.
887

888 Nørgaard-Pedersen, N., Spielhagen, R.F., Erlenkeuser, H., Grootes, P.M., Heinemeier,
889 J., Knies, J., 2003. Arctic Ocean during the Last Glacial Maximum: Atlantic and polar
890 domains of surface water mass distribution and ice cover. *Paleoceanography* 18,
891 doi:10.1029/2002PA000781, 2003.
892

893 Perner, K., Moros, M., Jennings, A., Lloyd, J.M., Knudsen, K.L., 2012. Holocene
894 palaeoceanographic evolution off West Greenland. *The Holocene* 23, 374-387.
895

896 Piénkowski, A.J., England, J.H., Furze, M.F.A., Marret, F., Eynaud, F., Vilks, G., Maclean,
897 B., Blasco, S., Scourse, J.D., 2012. The deglacial to postglacial marine environments of
898 SEBarrow Strait, Canadian Arctic Archipelago. *Boreas* 41 (2), 141-179.
899 <http://dx.doi.org/10.1111/j.1502-3885.2011.00227.x>.
900

901 Polyak, L., Korsun, S., Febo, L.A., Stanovoy, V., Khusid, T., Hald, M., Paulsen, B.E.,
902 Lubinski, D.J., 2002. Benthic foraminiferal assemblages from the southern Kara Sea,

903 a river influenced Arctic marine environment. *Journal Foraminiferal Research* 32,
904 252–273.

905

906 Post, A.L., Galton-Fenzi, B.K., Riddle, M.J., Herraiz-Borreguero, L., O'Brien, P.E.,
907 Hemer, M.A., McMinn, A., Rasch, D., Craven, M., 2014. Modern sedimentation,
908 circulation and life beneath the Amery Ice Shelf, East Antarctica. *Continental Shelf*
909 *Research* 74. 77-87.

910

911 Quillmann, U., Andrews, J. T., and Jennings, A. E., 2009: *Radiocarbon Date List XI:*
912 *East Greenland shelf, West Greenland Shelf, Labrador Sea. Baffin Island shelf, Baffin*
913 *Bay, Nares Strait, and Southwest to Northwest Icelandic shelf.* Occasional Paper No.
914 59, INSTAAR, University of Colorado, Boulder, Boulder.

915

916 Ramsey, C.B. and Lee, S., 2013. Recent and planned developments of the program
917 OxCal. *Radiocarbon* 55, 720-730.

918

919 Reeh, N., Thomsen, H. H., Higgins, A. K., and Weidick, A., 2001: Sea ice and the
920 stability of north and northeast Greenland floating glaciers. *In* Jeffries, M. O. and
921 Eicken, H. (eds.), *Annals of Glaciology, Vol 33*, 474-480.

922

923 Reimer, P.J., Bard, E., Bayliss, A., Beck, J.W., Blackwell, P.G., Ramsey, C.B., Grootes,
924 P.M., Guilderson, T.P., Hafliðason, H., Hajdas, I., Hatté, C., Heaton, T.J., Hoffmann,
925 D.L., Hogg, A.G., Hughen, K.A., Kaiser, K.F., Kromer, B., Manning, S.W., Niu, M.,
926 Reimer, R.W., Richards, D.A., Scott, E.M., Southon, J.R., Staff, R.A., Turney, C.S.M.,
927 van der Plicht, J., 2013. IntCal13 and Marine13 radiocarbon age calibration curves 0-
928 50,000 years cal BP. *Radiocarbon* 55, 1869–1887. [http://dx.doi.org/10.2458/azu_js_rc.](http://dx.doi.org/10.2458/azu_js_rc.55.16947)
929 55.16947.

930

931 Reineck, H.E., Singh, I.B., 1980. *Depositional Sedimentary Environments*. Springer-
932 Verlag, NY.

933

934 Sarnthein, M., et al., Variations in Atlantic surface ocean paleoceanography, 50_–80_N:
935 A time-slice record of the last 30,000 years, *Paleoceanography*, 10(6), 1063– 1094, 1995.

936 Schafer, C.T., Cole, F.E., 1988. Environmental associations of Baffin Island fjord
937 agglutinated foraminifera. *Abh. Geol. Bundesanst*, 307.

938

939 Seidenkrantz, M.-S., 2013. Benthic foraminifera as palaeo sea-ice indicators in the
940 subarctic realm-examples from the Labrador Sea-Baffin Bay region. *Quaternary Science*
941 *Reviews* 79, 135-144. <http://dx.doi.org/10.1016/j.quascirev.2013.03.014>

942

943 Shaffer, G., Olsen, S.M., Bjerrum, C.J., 2004. Ocean subsurface warming as a
944 mechanism for coupling Dansgaard-Oeschger climate cycles and ice-rafting events.
945 *Geophysical Research Letters* 31, L24202. doi:10.1029/2004GL020968.

946

947 Sheldon, C., Jennings, A., Andrews, J.T., Ó Cofaigh, C., Hogan, K., Dowdeswell, J.A.,
948 Seidenkrantz, M-S., 2016. Ice stream retreat following the LGM and onset of the west

949 Greenland current in Uummannaq Trough, west Greenland. *Quaternary Science Reviews*,
950 <http://dx.doi.org/10.1016/j.quascirev.2016.01.019>
951

952 Simon, Q., Hillaire-Marcel, C., St-Onge, G., Andrews, J.T., 2014. Northeastern
953 Laurentide, western Greenland and southern Innuitian ice stream dynamics during the last
954 glacial cycle. *Journal of Quaternary Science* 29(1): 14-26. DOI: 10.1002/jqs.2648
955

956 Simon Q, St-Onge G, Hillaire-Marcel C., 2012. Late Quaternary chronostratigraphic
957 framework of deep Baffin Bay glaciomarine sediments from high-resolution
958 paleomagnetic data. *Geochemistry, Geophysics, Geosystems* 13: Q0AO03. doi: 10.1029/
959 2012GC004272
960

961 Simon, Q., Thouveny, N., Bourles, D.L., Nuttin, L., Hillaire-Marcel, C., St-Onge, G.,
962 2016. Authigenic $^{10}\text{Be}/^9\text{Be}$ ratios and ^{10}Be -fluxes ($^{230}\text{Th}_{\text{xs}}$ -normalized) in central Baffin
963 Bay sediments during the last glacial cycle: Paleoenvironmental implications. *Quaternary*
964 *Science Reviews* 140, 142-162.
965

966 Slabon, P., Dorschel, B., Jokat, W., Myklebust, R., Hebbeln, D., Gebhardt, C., 2016.
967 Greenland ice sheet retreat history in the northeast Baffin Bay based on high-resolution
968 bathymetry. *Quaternary Science Reviews* 154, 182-198.
969 <http://dx.doi.org/10.1016/j.quascirev.2016.10.022>
970

971 Slubowska, M.A., Koç, N., Rasmussen, T.L., Klitgaard-Kristensen, D., 2005. Changes in
972 the flow of Atlantic water into the Arctic Ocean since the last deglaciation: evidence from
973 the northern Svalbard continental margin, 80°N. *Paleoceanography* 20, PA4014.
974 doi:10.1029/2005PA001141.
975

976 Stern, J.V., Lisiecki, L.E. 2013. North Atlantic circulation and reservoir age changes over
977 the past 41,000 years. *Geophysical Research Letters* 40: 3693-3697.
978 doi:10.1002/grl.50679, 2013.
979

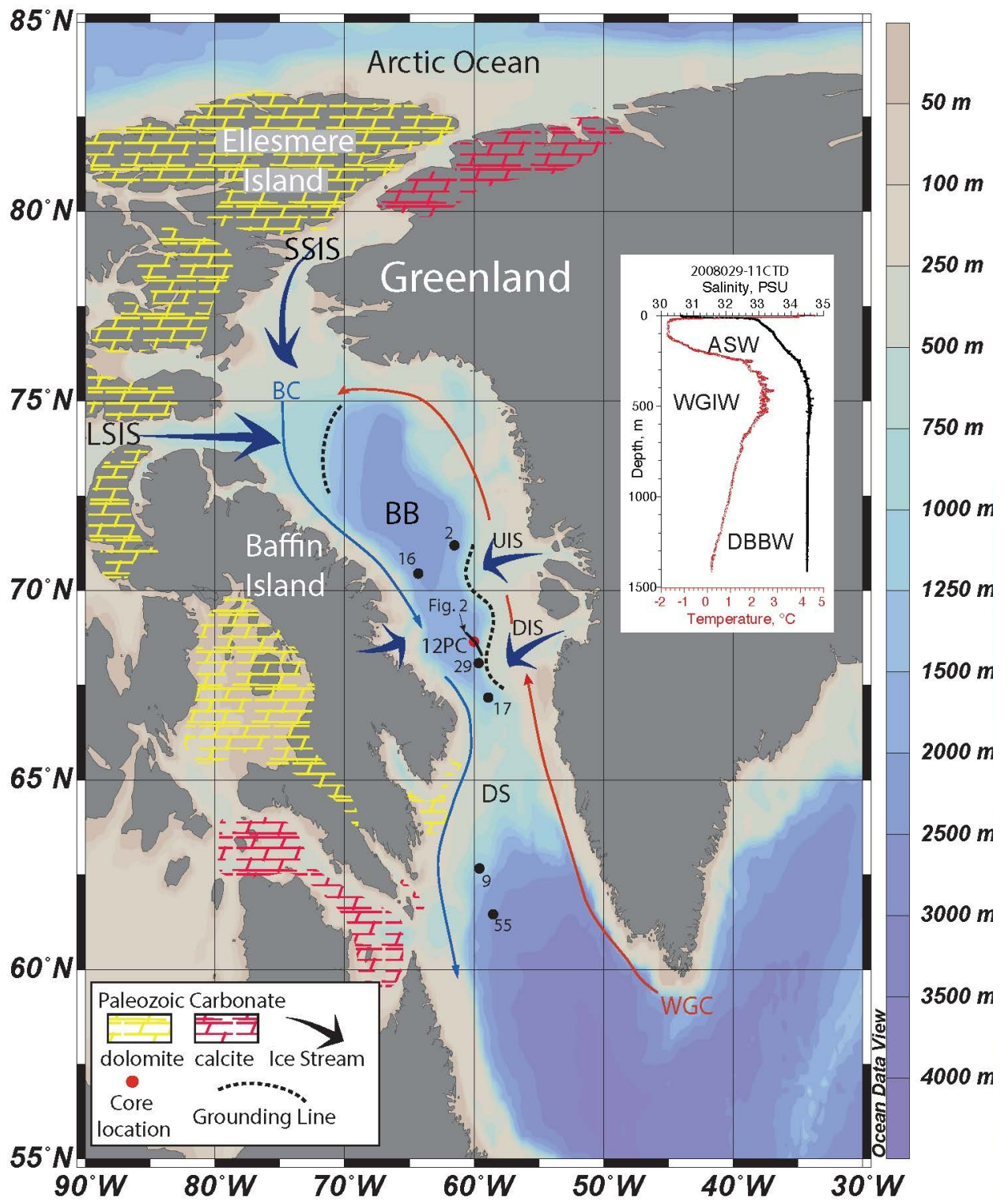
980 Straneo, F., Sutherland, D.A., Holland, D., Gladish, C., Hamilton, G.S., Johnson, H.L.,
981 Rignot, E., Xu, Y., Koppes, M., 2012. Characteristics of ocean waters reaching
982 Greenland's glaciers. *Annals of Glaciology* 53(60), 202-210.
983 doi:10.3189/2012AoG60A059
984

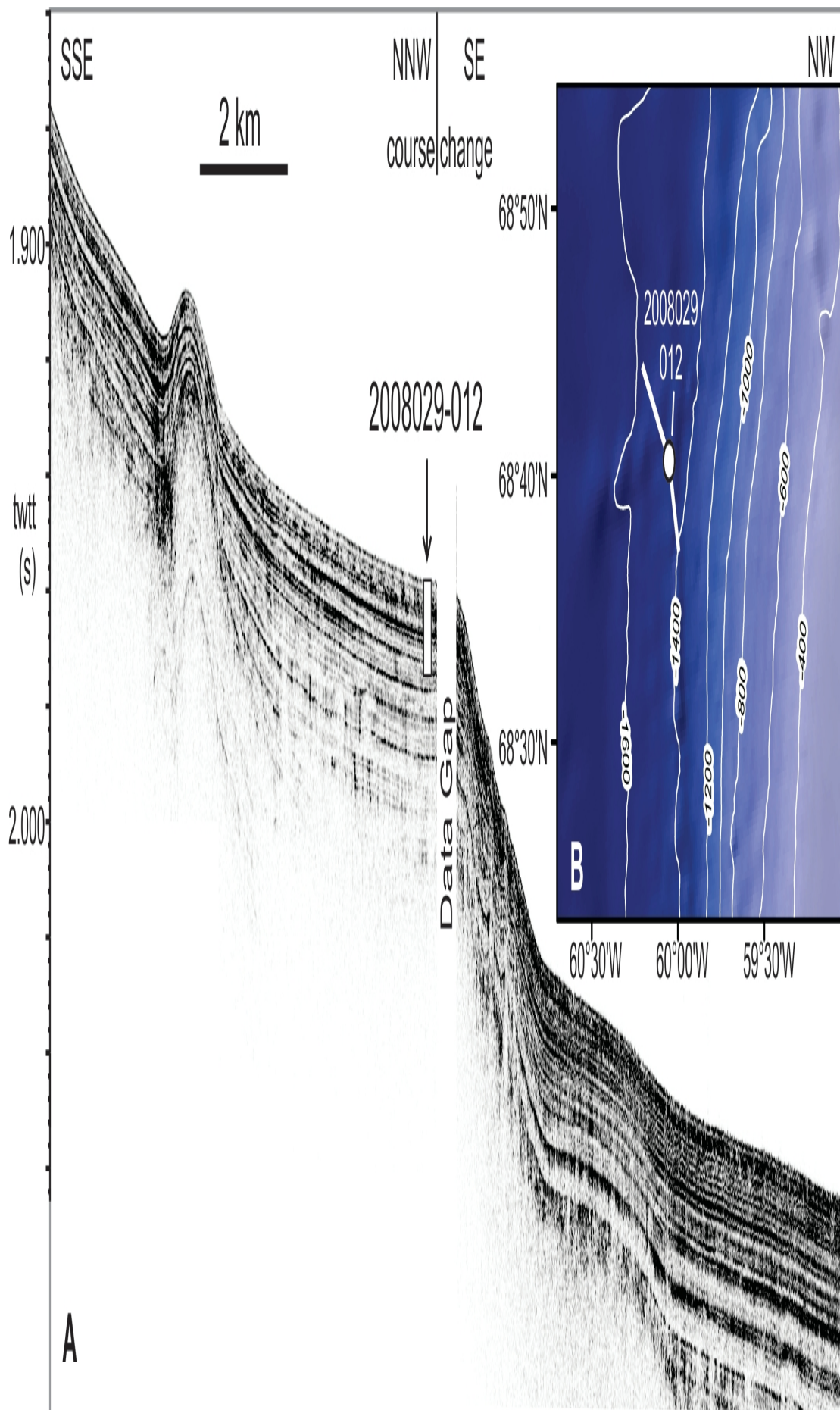
985 Tang, C.C.L., Ross, C.K., Yao, T., Petrie, B., DeTracey, B.M., Dunlap, E., 2004. The
986 circulation, water masses and sea-ice of Baffin Bay. *Progress in Oceanography* 63, 183–
987 228.
988

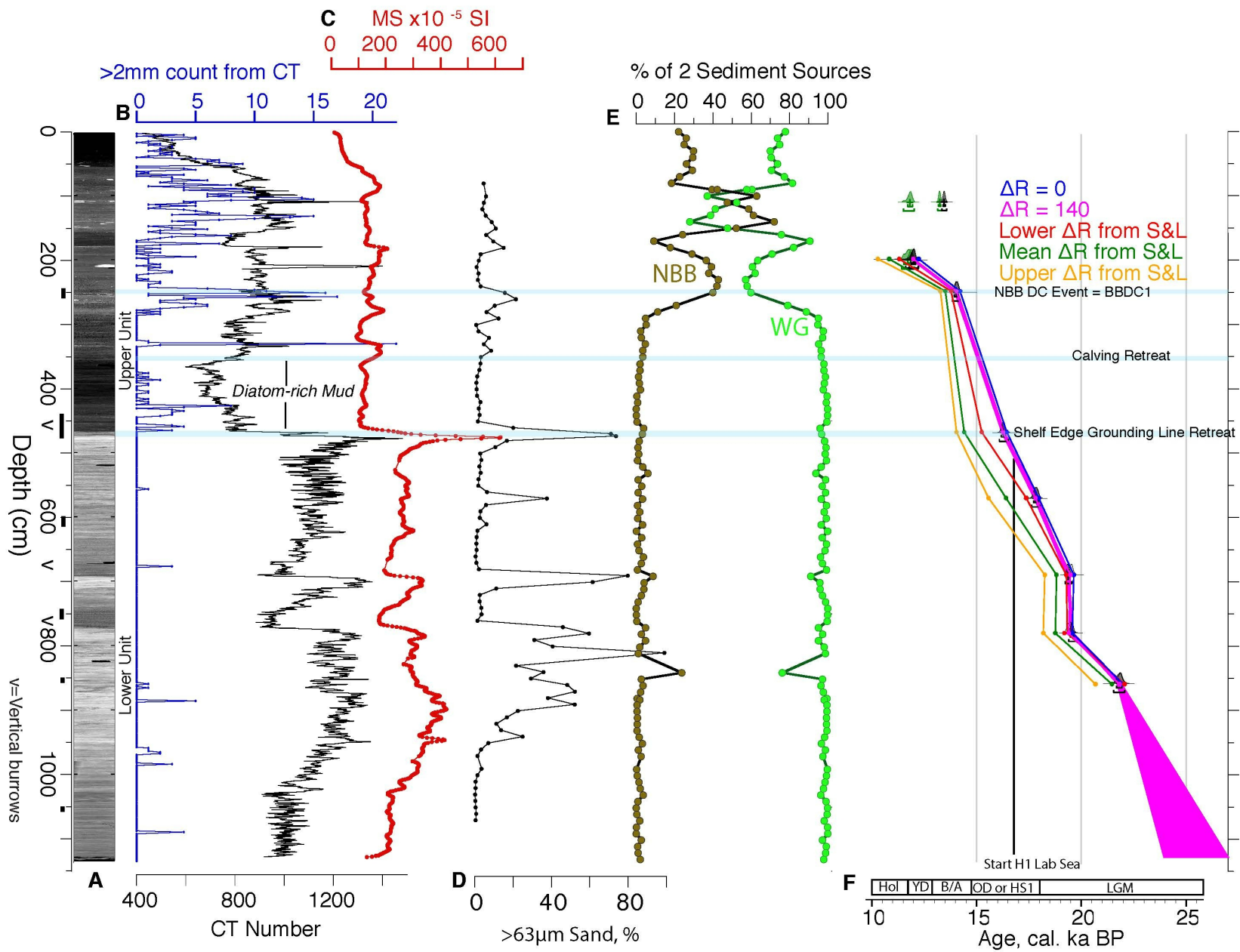
989 Wetzel, A., 1991. Ecologic interpretation of deep-sea trace fossil communities.
990 *Palaeogeography, Palaeoclimatology, Palaeoecology* 85, 47-69.
991

992 Wollenburg, J.E., Knies, J., Mackensen, A., 2004. High-resolution paleoproductivity
993 fluctuations during the past 24 kyr as indicated by benthic foraminifera in the

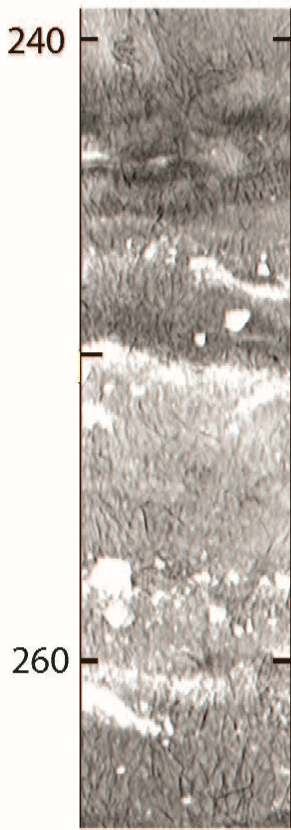
994 marginal Arctic Ocean. *Palaeogeography, Palaeoclimatology, Palaeoecology* 204, 209-
995 238.
996
997 Xiao, X., Fahl, K., Stein, R., 2013. Biomarker distributions in surface sediments from the
998 Kara and Laptev seas (Arctic Ocean): indicators for organic-carbon sources and sea ice
999 coverage. *Quaternary Science Reviews* 79, 40–52.
1000
1001 Zreda, M., J. England, F. Phillips, D. Elmore, and P. Sharma. 1999. Unblocking of the
1002 Nares Strait by Greenland and Ellesmere Ice-Sheet retreat 10,000 years ago. *Nature*
1003 398,139–142, <http://dx.doi.org/10.1038/18197>
1004



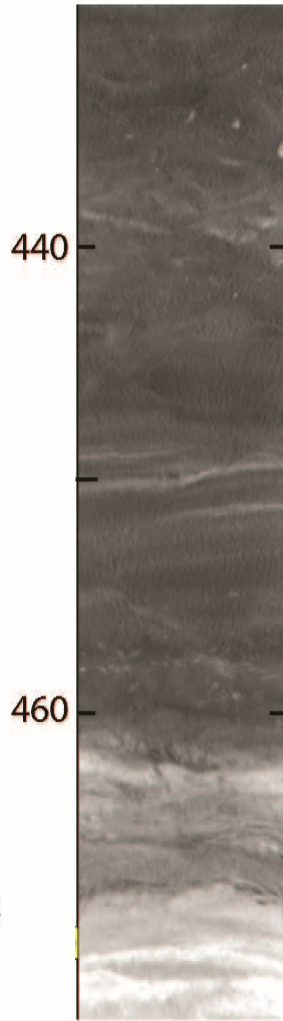




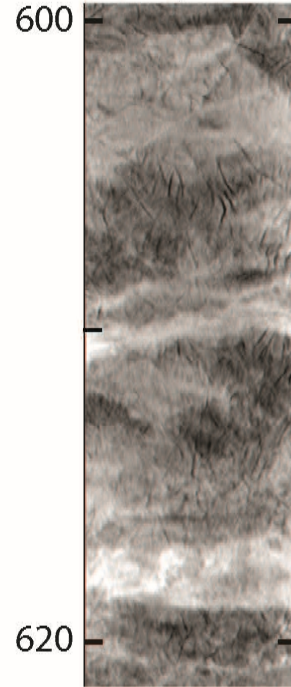
a. DC/IRD Event



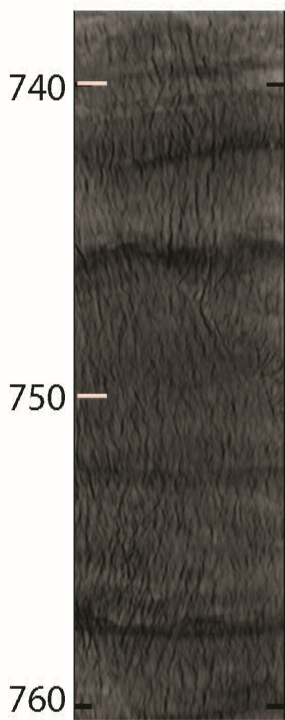
b. Transition



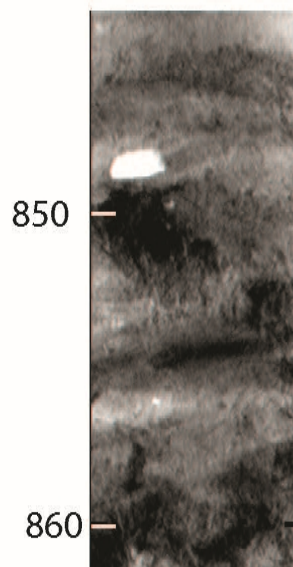
c. Bioturbated mud w/
Sand layers



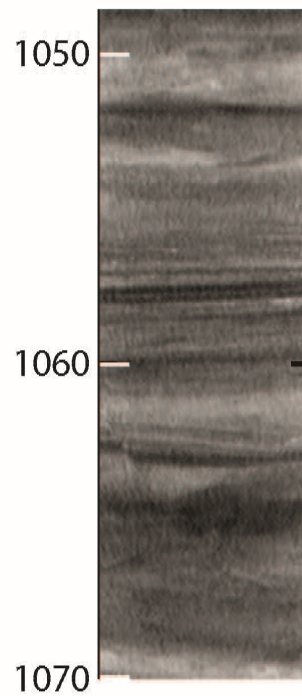
d. Stratified mud
w/ Vertical burrows

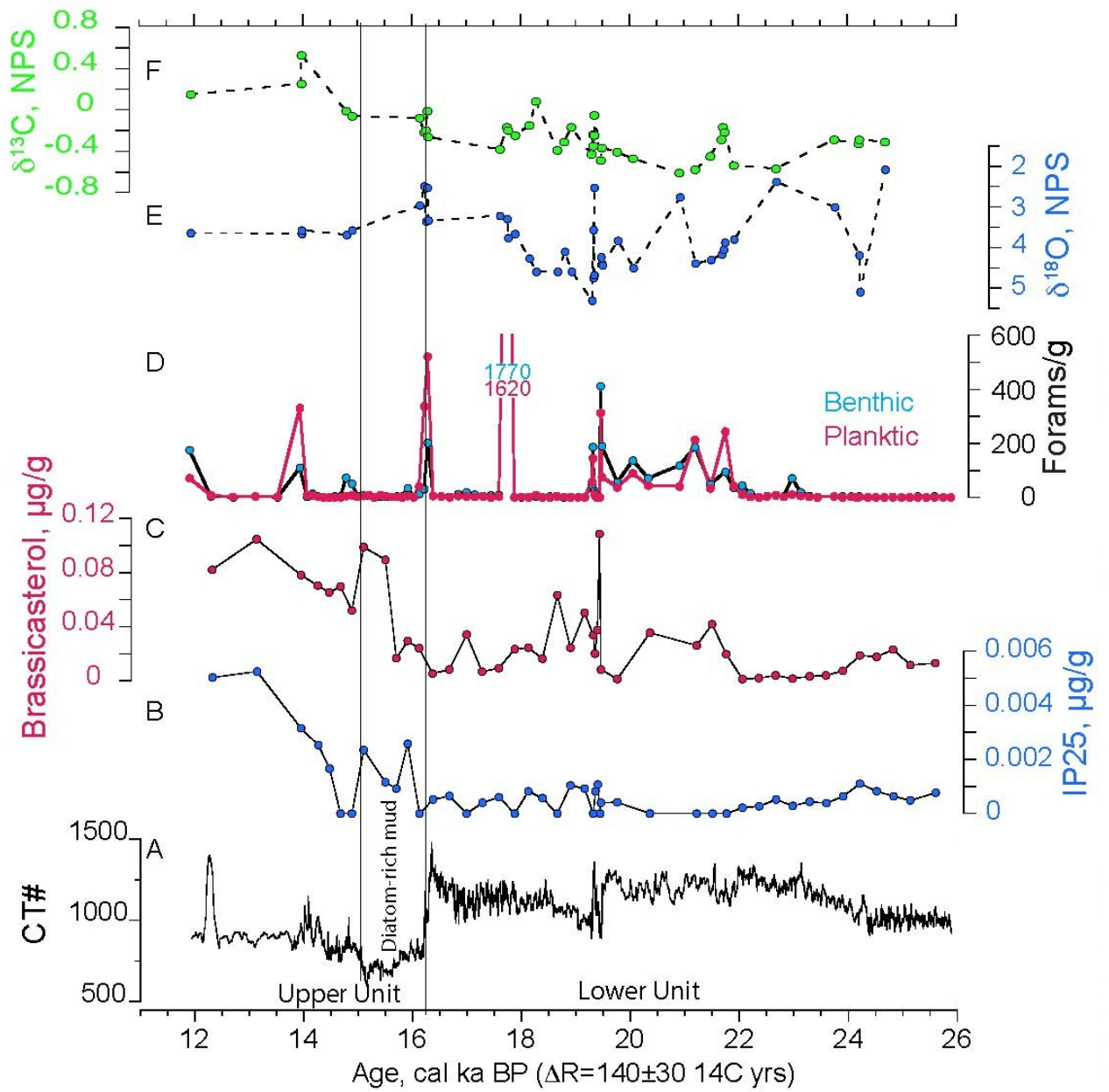


e. Bioturbated sandy
mud w/rare IRD

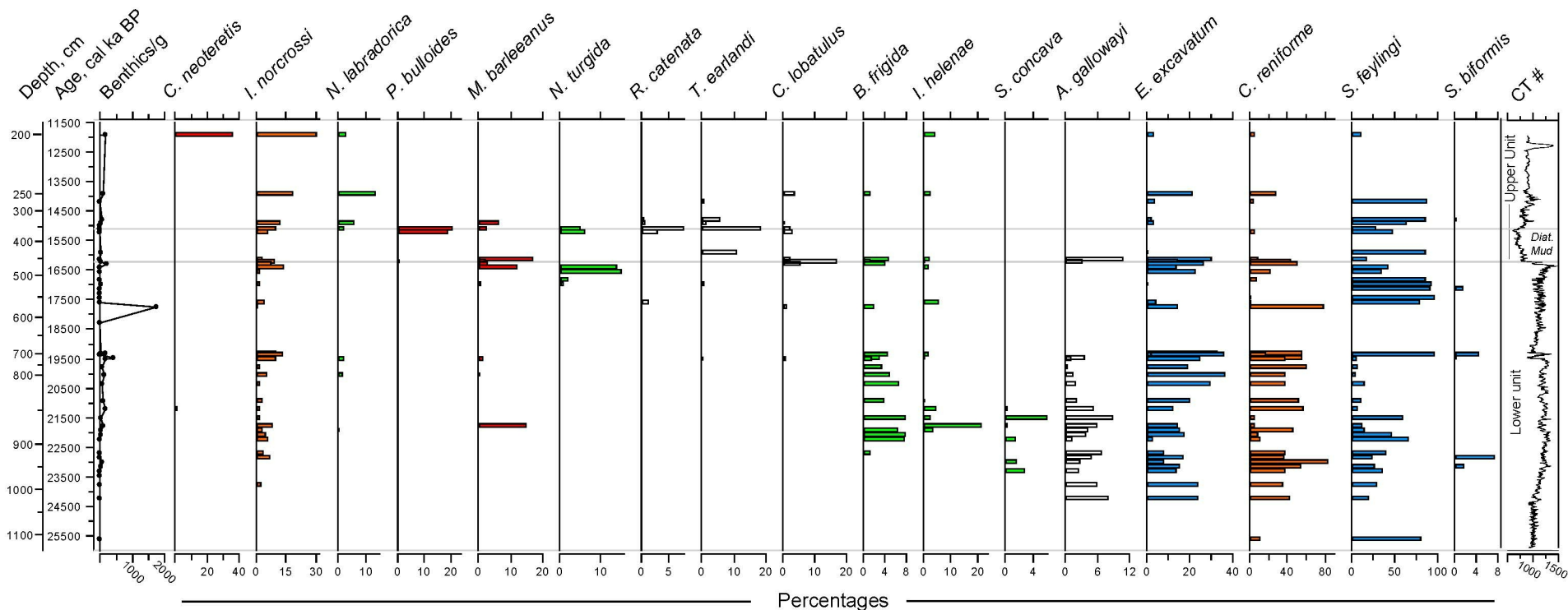


f. Stratified sand w/
bioturbation





HU2008029-12PC Benthic Foraminifera



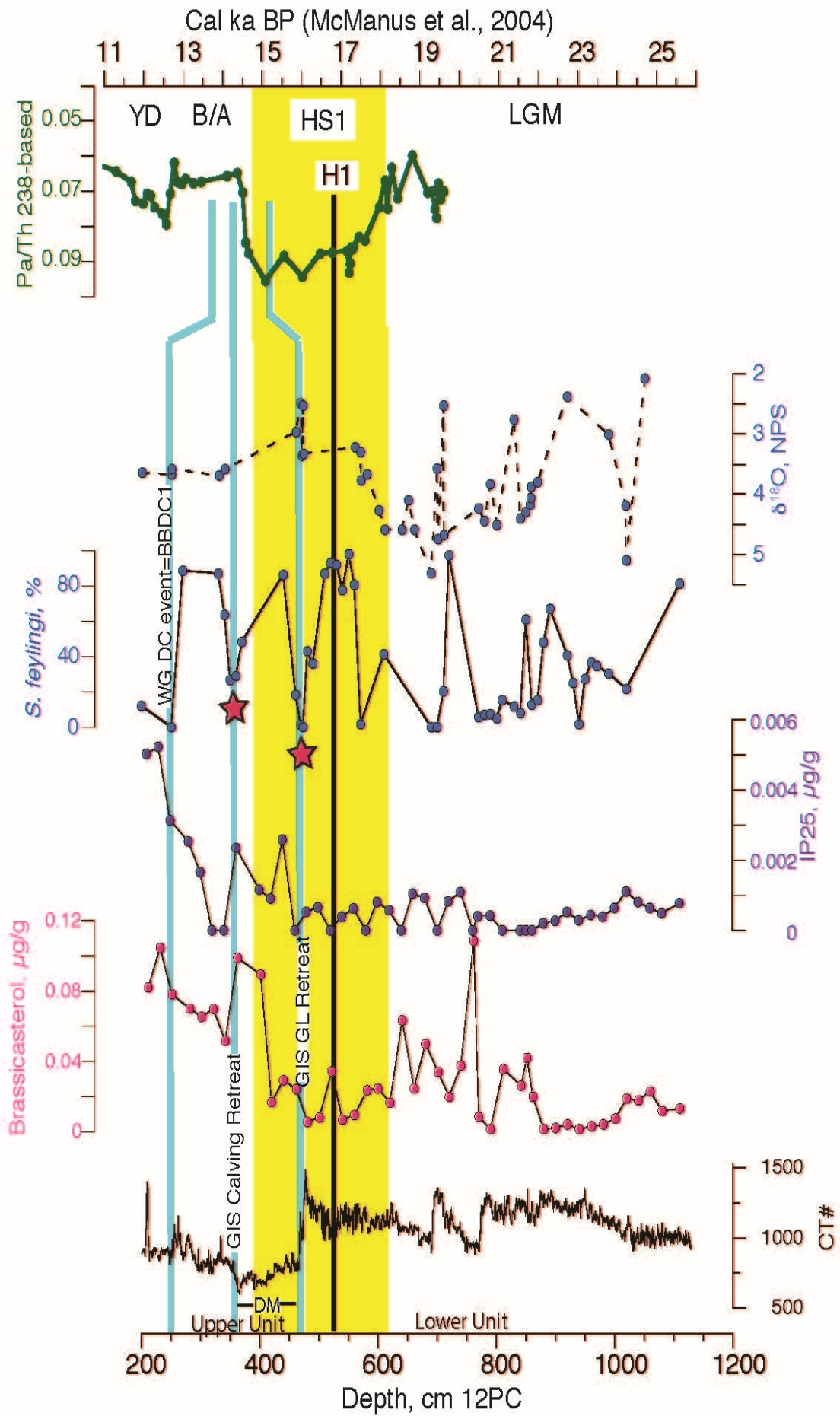


Table 1. Radiocarbon ages and their calibrations with varying ΔR .

HU2008029-12PC

Date	Depth	^{14}C	error	ΔR	Date (^{14}C age)
CURL14065	201.5	10760	35		0 CURL14065 with
CURL14065	201.5	10760	35		140 CURL14065 with
CURL14065	201.5	10760	35		470 CURL14065 with
CURL14065	201.5	10760	35		900 CURL14065 with
CURL14065	201.5	10760	35		1340 CURL14065 with
AA90386	251.5	12666	61		0 AA90386 with
AA90386	251.5	12666	61		140 AA90386 with
AA90386	251.5	12666	61		380 AA90386 with
AA90386	251.5	12666	61		630 AA90386 with
AA90386	251.5	12666	61		900 AA90386 with
CURL16671	469.5	14030	40		0 CURL16671 with
CURL16671	469.5	14030	40		140 CURL16671 with
CURL16671	469.5	14030	40		850 CURL16671 with
CURL16671	469.5	14030	40		1260 CURL16671 with
CURL16671	469.5	14030	40		1500 CURL16671 with
CURL18165	571.5	15150	60		0 CURL18165 with
CURL18165	571.5	15150	60		140 CURL18165 with
CURL18165	571.5	15150	60		500 CURL18165 with
CURL18165	571.5	15150	60		1150 CURL18165 with
CURL18165	571.5	15150	60		1750 CURL18165 with
CURL14067	690.5	16660	45		0 CURL14067 with
CURL14067	690.5	16660	45		140 CURL14067 with
CURL14067	690.5	16660	45		290 CURL14067 with
CURL14067	690.5	16660	45		720 CURL14067 with
CURL14067	690.5	16660	45		1250 CURL14067 with
CURL16663	780.5	16600	50		0 CURL16663 with
CURL16663	780.5	16600	50		140 CURL16663 with
CURL16663	780.5	16600	50		290 CURL16663 with
CURL16663	780.5	16600	50		720 CURL16663 with
CURL16663	780.5	16600	50		1250 CURL16663 with
CURL18628	859.5	18540	80		0 CURL18628 with
CURL18628	859.5	18540	80		140 CURL18628 with
CURL18628	859.5	18540	80		-50 CURL18628 with
CURL18628	859.5	18540	80		420 CURL18628 with
CURL18628	859.5	18540	80		1010 CURL18628 with

Base of H1 ages from the Labrador Sea

HU87033-009 LCF, 500-501 cm; Jennings et al., 1996

AA-9364		14980	90		0 AA-9364 with
AA-9364		14980	90		140 AA-9364 with
AA-9364		14980	90		500 AA-9364 with

AA-9364	14980	90	1150 AA-9364 with
AA-9364	14980	90	1750 AA-9364 with

HU75009-IV-055PC, 115-117 cm; Kaufman and Williams, 1992

AA-5999	15010	105	0 AA-5999 with
AA-5999	15010	105	140 AA-5999 with
AA-5999	15010	105	500 AA-5999 with
AA-5999	15010	105	1150 AA-5999 with
AA-5999	15010	105	1750 AA-5999 with

Calibrated						
1sigma from	1sigma to	2sigma from	2sigma to	mean	error	
12306	12075	12430	12028	12215	109	
12026	11865	12100	11755	11937	86	
11317	11210	11432	11161	11282	70	
10868	10706	10972	10667	10805	79	
10291	10196	10373	10176	10260	51	
14279	14051	14542	13964	14208	142	
14095	13926	14165	13840	14007	83	
13845	13665	13930	13555	13748	91	
13552	13392	13657	13332	13484	81	
13312	13180	13375	13114	13246	66	
16511	16309	16632	16233	16423	102	
16311	16144	16424	16045	16232	90	
15282	15148	15375	15076	15221	73	
14507	14193	14701	14136	14398	155	
14086	13947	14143	13873	14011	68	
18035	17854	18130	17740	17941	94	
17887	17687	17973	17598	17785	97	
17465	17236	17549	17125	17345	110	
16491	16261	16631	16174	16390	117	
15680	15408	15776	15297	15541	128	
19698	19528	19832	19467	19631	91	
19550	19372	19609	19260	19449	88	
19368	19168	19466	19070	19268	99	
18850	18739	18905	18674	18791	57	
18328	18149	18395	18039	18226	90	
19634	19467	19749	19360	19553	91	
19480	19283	19560	19203	19380	93	
19257	19061	19385	18986	19177	99	
18802	18680	18856	18605	18735	62	
18267	18071	18337	17973	18160	94	
22113	21850	22271	21751	21993	131	
21916	21670	22057	21537	21795	127	
22175	21905	22301	21820	22051	128	
21594	21299	21746	21137	21442	149	
20772	20537	20913	20434	20662	119	

17878	17633	17984	17515	17752	120	
17725	17460	17883	17333	17599	136	
17281	16963	17437	16789	17115	161	

16288	16021	16449	15861	16155	140
15443	15143	15656	15041	15318	155
17916	17650	18037	17513	17780	133
17785	17490	17925	17345	17634	147
17345	17000	17495	16800	17156	174
16345	16032	16538	15875	16200	163
15528	15180	15733	15060	15367	174

median

12207

11943

11270

10796

10250

14180

14009

13751

13478

13246

16416

16230

15218

14378

14014

17943

17786

17349

16381

15544

19621

19455

19264

18793

18234

19551

19382

19173

18738

18163

21985

21798

22048

21444

20657

17753

17597

17115

16154
15302

17781
17633
17159
16195
15356
